Soil moisture profile estimation by combining P-band SAR polarimetry with hydrological and multi-layer scattering models

Anke Fluhrer, Thomas Jagdhuber, Carsten Montzka, Maike Schumacher, Hamed Alemohammad, Alireza Tabatabaeenejad, Harald Kunstmann, Dara Entekhabi

Angaben zur Veröffentlichung / Publication details:

Fluhrer, Anke, Thomas Jagdhuber, Carsten Montzka, Maike Schumacher, Hamed Alemohammad, Alireza Tabatabaeenejad, Harald Kunstmann, and Dara Entekhabi. 2024. "Soil moisture profile estimation by combining P-band SAR polarimetry with hydrological and multi-layer scattering models." *Remote Sensing of Environment* 305: 114067. https://doi.org/10.1016/j.rse.2024.114067.

Remote Sensing of Environment 305 (2024) 114067

Contents lists available at ScienceDirect

Remote Sensing of Environment

journal homepage: www.elsevier.com/locate/rse

Soil moisture profile estimation by combining P-band SAR polarimetry with hydrological and multi-layer scattering models

Anke Fluhrer [a,b,*], Thomas Jagdhuber [a,b], Carsten Montzka [c], Maike Schumacher [d], Hamed Alemohammad [e], Alireza Tabatabaeenejad [f], Harald Kunstmann [b,g], Dara Entekhabi [h]

[a] Microwaves and Radar Institute, German Aerospace Center (DLR), Muenchener Straße 20, 82234 Weßling, Germany
[b] Institute of Geography, University of Augsburg, Alter Postweg 118, 86159 Augsburg, Germany
[c] Institute of Bio- and Geosciences: Agrosphere (IBG-3), Forschungszentrum Juelich, Wilhelm-Johnen-Straße, 52428 Juelich, Germany
[d] Geodesy Group, Department of Planning, Aalborg University, Rendsburggade 14, 9000 Aalborg, Denmark
[e] Center for Geospatial Analytics & Graduate School of Geography, Clark University, Worcester, MA 01610, USA
[f] The Aerospace Corporation, El Segundo, CA 90245, USA
[g] Institute of Meteorology and Climate Research, Karlsruhe Institute of Technology, Kreuzeckbahnstraße 19, 82467 Garmisch-Partenkirchen, Germany
[h] Department of Civil and Environmental Engineering, Massachusetts Institute of Technology (MIT), Cambridge, MA 02139, USA

ARTICLE INFO

Edited by Jing M. Chen

Keywords:
AirMOSS
Hybrid polarimetric decomposition
HYDRUS-1D
Remote sensing

ABSTRACT

An approach for estimating vertically continuous soil moisture profiles under varying vegetation covers by combining remote sensing with soil (hydrological) modeling is proposed. The approach uses decomposed soil scattering components, after the removal of the vegetation scattering components from fully polarimetric P-band SAR observations. By comparing these with hydrological simulations, soil moisture profiles from the soil surface until a soil depth of 30 cm (assumed average P-band penetration depth) are estimated. Here, the hydrological model HYDRUS-1D, as a representative of any soil hydrological model, is employed to simulate an ensemble of realistic soil moisture profiles, which are used for a multi-layer soil scattering model to obtain forward modeled soil scattering components. Compared to the decomposed SAR-based soil scattering components, the most appropriate soil moisture profile from the ensemble is estimated. The approach is able to provide physically (hydraulic) more meaningful soil moisture profile shapes than currently existing profile estimation approaches, like polynomial fitting to few measurements at discrete soil depths. Results are presented across eight *in situ* measuring stations in the U.S. within six test sites of NASA's Airborne Microwave Observatory of Subcanopy and Subsurface (AirMOSS) mission between 2013 and 2015. In-depth analyzes and validations with *in situ* measured soil moisture information demonstrate the feasibility of the proposed approach. Overall, estimated soil moisture profiles at the different sites match the varying local climate, vegetation cover, and soil conditions. Coefficients of determination between estimated and *in situ* measured soil moisture values vary between 0.48 and 0.92, while unbiased errors range from 1.4 vol% to 3.7 vol%, and Fréchet distances (analyzing the similarity of profile shapes) vary between 0.1 and 0.2 [−].

1. Introduction

Although soil moisture as part of the geosphere accounts for only ~0.0089% of the total water on Earth (Dingman, 2015), it significantly contributes to the characterization of the Earth's climate (Bojinski et al., 2014). Soil moisture links exchanges between the land and the atmosphere, and connects the water and carbon cycles through evapotranspiration (Dingman, 2015). In weather forecasting and climate modeling, the soil moisture distribution and variability across the vertical soil column is evident since it has direct impact on land-atmosphere coupling, evapotranspiration as well as heat and water exchanges (Dingman, 2015; Dirmeyer et al., 2016; Feddes et al., 2001). For example, the current state of the soil moisture variability across the vertical soil column, the so-called soil moisture profile, controls how fast

* Corresponding author at: Microwaves and Radar Institute, German Aerospace Center (DLR), Muenchener Straße 20, 82234 Weßling, Germany.
E-mail addresses: Anke.Fluhrer@dlr.de (A. Fluhrer), Thomas.Jagdhuber@dlr.de (T. Jagdhuber), c.montzka@fz-juelich.de (C. Montzka), maikes@plan.aau.dk (M. Schumacher), halemohammad@clarku.edu (H. Alemohammad), alirezat@aero.org (A. Tabatabaeenejad), harald.kunstmann@kit.edu (H. Kunstmann), darae@mit.edu (D. Entekhabi).

https://doi.org/10.1016/j.rse.2024.114067
Received 16 May 2023; Received in revised form 25 January 2024; Accepted 17 February 2024
Available online 5 March 2024

water can infiltrate and percolate vertically through the soil as well as how quickly a soil dries out (Ford et al., 2014). Hence, it controls, for instance, crop and plant growth, soil erosion, landslides, and forest fires. Up to now, soil moisture and its vertical variability is mainly treated secondarily in climate modeling (Vereecken et al., 2022). However, several studies showed that unrealistic initial assumptions on soil moisture impact the forecast skill of models, stating that remotely sensed soil moisture can have great potential in improving climate modeling by describing the coupled land-atmosphere behavior more realistically (Dirmeyer et al., 2018; Koster et al., 2011). For instance, the second phase of the Global Land-Atmosphere Coupling Experiment (GLACE-2) was intended to investigate how more realistic land surface initializations, notably soil moisture, would improve the forecast skill of climate models. Results showed that in many regions realistic initializations, for example from remotely sensed soil moisture observations, can significantly improve this skill (Koster et al., 2011).

Up to now, remote sensing approaches allow the estimation of soil moistures at the soil surface from L-band measurements (He et al., 2016; Jagdhuber et al., 2015), or at deeper soil depths within the root zone from P-band measurements (Etminan et al., 2020; Fluhrer et al., 2022; Tabatabaeenejad et al., 2015). These approaches represent the behavior of moisture across the soil profile from the soil surface until the sensing depth of the microwave with just one single uniform value. Estimating only single soil moisture values from few radar measurements, however, is prone to errors and often impractical due to the high number of unknowns compared to the available number of measurements (Konings et al., 2014).

Further, the soil moisture variability with depth cannot be estimated from single remote sensing observations despite the fact that the radar backscatter is able to provide information about soil moisture discontinuities. However, knowledge about the soil moisture profile is of utmost importance in climate research and many environmental applications, like land surface, weather and climate monitoring (Walker et al., 2001), or agricultural production and food security (Almendra-Martín et al., 2021).

There already exist different approaches to estimate soil moisture profiles by using land surface modeling or remote sensing data assimilation techniques. The simplest approach to estimate a soil moisture profile is from soil moisture information at discrete soil depths by fitting a polynomial function of certain degree through the few known points. The soil moisture information for that can originate from *in situ* field measurements, L- and P-band remote sensing techniques, or from models. Overall, the polynomial approach is rather imprecise and physically less robust since this mathematical assumption on very few, sometimes just three moisture values, can only represent high level simplifications of the reality, although there are recent attempts to improve the polynomial soil moisture profile estimation, *e.g.*, (Sadeghi et al., 2016). Further, attempts have been made to retrieve RZSM values from prognostics describing the 'average deviations from the equilibrium profile' (Reichle et al., 2017), or by evaluating the degree of association or coupling strength between near surface and *in situ* root zone soil moistures, *e.g.*, (Ford et al., 2014; Short Gianotti et al., 2019). Here, assumptions on theoretical relationships ignore the lack of transferability of soil moisture dynamics across spatio-temporal scales. However, soil moisture in the subsurface responds slower to changes and is less variable compared to near-surface soil moisture (Ford et al., 2014; Short Gianotti et al., 2019). This means, the link between both is highly complex especially after a precipitation event. Another method for soil moisture profiles estimation is the comparison of the observed backscatter from radars with simulated backscatters based on forward models (Konings et al., 2014). However, a radar signal includes all potential scattering mechanisms from soil, vegetation, and the combination of both. Hence, the vegetation volume covering the soil also has to be modeled and considered in backscatter simulations, which requires certain assumptions and adds additional complexity to the modeling. Lastly, several soil moisture approaches have been published based on land data assimilation. For that, spatially or temporally coarse soil moisture *in situ* measurements or satellite-derived soil moisture information are used in a land surface model together with auxiliary information, such as precipitation or soil characteristics. In this way, enhanced model calibration, spatially or temporally upscaled soil moisture information, or RZSM estimates across the vertical soil profile can be achieved (Lei et al., 2020; Liu et al., 2011; Tangdamrongsub et al., 2020). The advantages of the proposed approach compared to assimilation are, for one, that no prior information on soil moisture conditions across the vertical soil profile has to be known, neither from *in situ* measurements, nor satellite-derived. Second, no dense time series of remote sensing observations is required as input, as the comparison of decomposed P-band SAR data and model simulations can be done for every time step individually. However, assimilating temporally coarse remote sensing data, as available from the AirMOSS mission (~4–5 dates per year), is not sufficient enough for valid results. Lastly, the decomposed remote sensing estimate can be compared directly with model simulations without the need for model adaptions.

Besides remote sensing, soil states, like soil moisture, can be modeled with hydrological models based on measured atmospheric (*e.g.* precipitation, solar radiation, wind speed) and soil (*e.g.* temperature, matric potential, conductivity) parameters. In hydrological modeling, one of the general equations for predicting and describing one-dimensional water movement in (partially) saturated or unsaturated soils is the well-known Richards equation (Dingman, 2015), a combination of the mass conservation law (continuity principle) and the Darcy-Buckingham equation (Sadeghi et al., 2016). The Richards equation is a partial differential and highly nonlinear equation due to the dependence of the hydraulic conductivity and the soil water content on the soil matric potential. This means, a closed-form analytical solution of the equation is impossible, except for special cases with many simplifications and certain boundary conditions (Dingman, 2015). However, these can only lead to approximate solutions and are not generally applicable. There exist many hydrological models to numerically solve the Richards equation by either employing "a finite difference, finite volume, or finite element approximation in space" (Farthing and Ogden, 2017), *e.g.*, the Flux-Penn State Integrated Hydrologic Model (Shi et al., 2013), the ParFlow (Ashby and Falgout, 1996), or the RichardsFOAM (Orgogozo et al., 2014).

In this study, a joint approach of remote sensing and soil hydrological modeling is proposed for the estimation of continuous soil moisture profiles. The approach compares decomposed polarimetric P-band SAR estimates with respective simulations from the HYDRUS-1D (soil hydraulic model). The advantage of the proposed approach is, for one, that vegetation scattering contributions to the total SAR signal are removed before the comparison. Second, unlike in standard hydrological modeling, less assumptions on initial conditions are made in order to decrease potential sources for errors within simulations. That way, the proposed approach allows the comparison of actual observed SAR measurements with a set of hydrological simulations in order to estimate the most probable soil moisture profile.

The approach is supposed to lead to physically (hydraulic) more meaningful soil moisture profile shapes than mathematical approximations like polynomial fittings. Further, it provides the advantage of estimating continuous soil moisture profiles under varying vegetation covers (from grassland to forests) and for different climates.

2. Data sources

In this study, the polarimetric P-band SAR dataset from the Airborne Microwave Observatory of Subcanopy and Subsurface (AirMOSS) campaign, compiled between 2012 and 2015 by the National Aeronautics and Space Administration (NASA), is used. During the AirMOSS campaign, fully polarimetric SAR signals at a center frequency of 430 MHz, with a high radiometric calibration accuracy of 0.5 dB, and a noise equivalent of −40 dB were recorded across ten sites in Northern and

Central America. It was the first P-band airborne mission fully dedicated to RZSM estimation. Each monitoring site was revisited at least three times every campaign year and covers an area of ~25 × 100 km at ~90 m spatial resolution (Alemohammad et al., 2018). Detailed information on the campaigns and the instrument can be found in, *e.g.*, (Alemohammad et al., 2018; Chapin et al., 2012).

The proposed approach is validated and analyzed thoroughly with comparison to *in situ* field measurements. The focus in this study is on SAR pixels (where *in situ* data from measuring stations are available) within six AirMOSS sites in the U.S. (Fig. 1). These sites are "Howland Forest" in Maine, "Duke Forest" in North Carolina, "Metolius" in Oregon, "MOISST" in Oklahoma, "Tonzi Ranch" in California, and "Walnut Gulch" in Arizona. Information and locations on the investigated AirMOSS monitoring sites and the *in situ* measuring stations are shown in Fig. 1 and Table 1.

Fig. 1 shows that two sites are located at the east and three sites on the west coast of the U.S., with one site in the center. Hence, the climate regimes vary between cold humid continental climate with warm summers and significant precipitation in all seasons (Dfb), temperate climate with mild, dry, or hot summers (Csa, Csb, Cfa), and arid climate of a desert with warm summers (BSk) (Peel et al., 2007).

The soil textures indicate different types of a loamy soil (Fig. 1), while the landcover classes vary from grasslands, pastures or shrublands of woody savannas (with forest canopy cover between 30 and 60% and forest height exceeding 2 m) to evergreen needleleaf forests (Homer et al., 2015). Further, the amount of available dates for every AirMOSS site, where SAR measurements were recorded, vary between 13 and 22, with three to ten dates per year (in total 143 dates) (Table 1).

For hydrological simulations of soil moisture profiles (see Sec. 3.2.), input parameters from *in situ* measuring stations of the AmeriFlux network (AmeriFlux, 2022) and the US Climate Reference Network (USCRN) (Bell et al., 2013) are used. For the subsequent validation of results, soil moisture measurements at multiple depths from the same *in situ* networks are used (Fig. 1, Table 1). The focus in this study is on presenting and validating the proposed method for estimation of continuous soil moisture profiles from combined P-band polarimetry and soil modeling. Nevertheless, obtained results are additionally compared to two well-known soil moisture products: the European ReAnalysis (ERA5) land product from the European Centre for Medium-Range Weather Forecasts (ECMWF) (Muñoz Sabater, 2019), and the project AirMOSS L4 mission product (Crow et al., 2016). The ERA5-land dataset is a reanalysis product combining available observations with model data based on physics. The core is the Carbon Hydrology-Tiled ECMWF Scheme for Surface Exchanges over Land (CHTESSEL). For the ERA5-land soil moisture, for example, a total of >800 *in situ* sensors from various networks around the globe are used to initialize the model (Muñoz-Sabater et al., 2021). In contrast, the AirMOSS L4 product is based on mathematically integrating (polynomials) the AirMOSS L2/L3 product (Moghaddam et al., 2016), which provides soil moisture estimates at specific depths by using the AirMOSS P-band SAR observations along with several models (vegetation, ground surface scattering, subsurface scattering), with the Penn State Integrated Hydrologic Model (PIHM) and auxiliary information (*e.g.*, land cover classes, soil texture) (Crow et al., 2016). However, no in-depth comparison of the different methods for soil moisture estimation is performed and could be done in a follow-on study, outlining in detail the differences in algorithms, and consequently, results.

3. Methods

In this study, a combined technique of remote sensing and soil hydrological modeling is proposed for estimating continuous soil moisture profiles. As outlined in Fig. 2, the polarimetric soil scattering angle α_s^{SAR} can be determined from radar remote sensing, by decomposing the observed SAR signals into the individual scattering mechanisms (soil, dihedral, and volume) (Fluhrer et al., 2022).

From hydrological modeling, simulated soil moisture profiles θ_{SMPn} from HYDRUS-1D can be used as input to the multi-layer small perturbation method (SPM) (Tabatabaeenejad and Moghaddam, 2006) to forward model the backscatter coefficients from several soil layers, and calculate their polarimetric soil scattering angle $\alpha_s^{Model}n$. In the end, the soil moisture profile is estimated from the best fit between α_s^{SAR} and all $\alpha_s^{Model}n$.

Here, the comparison between decomposed SAR data and forward simulations is performed on the level of the polarimetric soil scattering angle α_s instead of directly comparing the observed and modeled backscatter coefficients. One reason is, that the observed backscatter coefficients contain scattering from all mechanisms (soil, dihedral, volume) and not only soil scattering. Another reason is that from remote sensing fully polarimetric backscatter coefficients are available, while from electromagnetic forward modeling only co-polarized (HH, VV) backscatter coefficients are obtainable. Hence, the use of α_s^{SAR} after the decomposition ensures remotely sensed information from the soil scattering component only but without loss on information since all observed co- and cross-polarized (HH, VV, HV, VH) backscatter coefficients are used within the decomposition.

It is important to emphasize that soil hydrological modeling does not simulate backscatters. A hydrological model (in this study the HYDRUS-1D) is used to compute soil moisture profiles, which in turn are used for backscatter simulations based on an electromagnetic model, in this study the multi-layer SPM.

In the following, both procedures to estimate the respective soil scattering angle α_s and the joint technique will be described in more detail.

3.1. Decomposed polarimetric soil scattering angle from P-band SAR observations

The polarimetric soil scattering angle α_s^{SAR} is estimated by decomposing the observed P-band SAR signal into individual scattering components by applying the hybrid decomposition method from (Fluhrer et al., 2022). This method separates the reflection symmetric, polarimetric coherency matrix $[T]$ from observed SAR signals into the three scattering components (surface $[T_s]$, dihedral $[T_d]$, and volume $[T_v]$):

$$\begin{bmatrix} T_{11} & T_{12} & 0 \\ T_{12}^* & T_{22} & 0 \\ 0 & 0 & T_{33} \end{bmatrix} = [T_s] + [T_d] + [T_v], \tag{1}$$

where T_{12}^* is the complex conjugate (Fluhrer et al., 2022). The volume component is defined by

$$[T_v] = \frac{f_v}{2 + 2A_p^2} \begin{bmatrix} V_{11} & V_{12} & 0 \\ V_{12}^* & V_{22} & 0 \\ 0 & 0 & V_{33} \end{bmatrix}, \tag{2}$$

where f_v is the volume scattering intensity, A_p $[-]$ is the particle anisotropy, and V_{xx} $[-]$ are the parameters to estimate the volume component. The V_{xx} parameters are based on A_p and the width of the orientation angle distribution $\Delta\psi$, describing 'the degree of orientation of the vegetation volume from oriented ($\Delta\psi = 0°$) to random ($\Delta\psi = 90°$)' (Fluhrer et al., 2022). Similar to the study of (Fluhrer et al., 2022), realistic parameter spaces for both variables are used, with $A_p \in [0, 1]$ and $\Delta\psi \in [0°, 90°]$. Further, all $A_p - \Delta\psi$ combinations leading to negative powers are excluded in further analyses. This way, multiple, valid vegetation representatives ensure an improved removal of the vegetation component. Lastly, the eigen-based soil scattering angle α_s^{SAR} can be estimated:

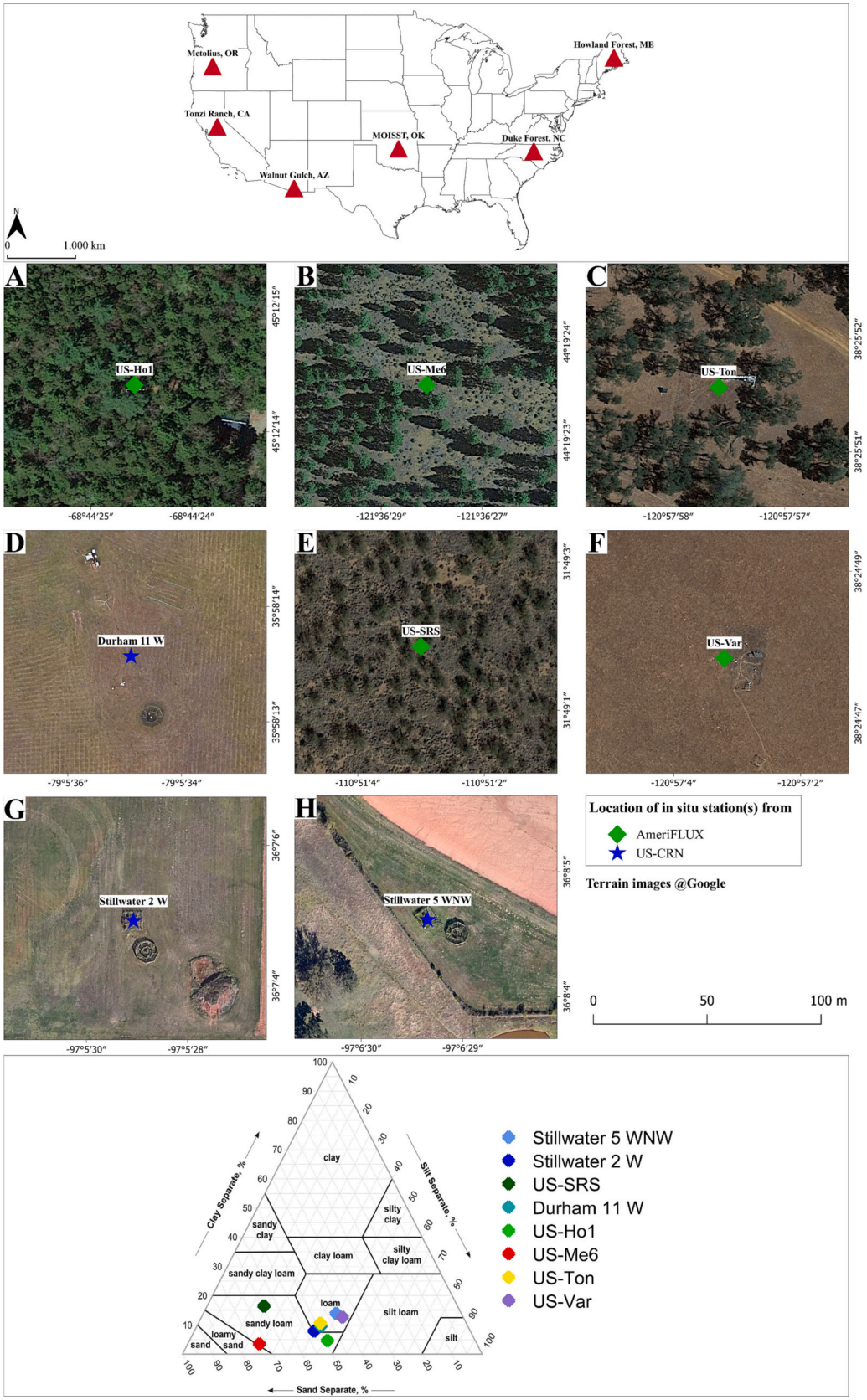

Fig. 1. Overview of employed *in situ* measuring stations at AirMOSS monitoring sites in the U.S.: (A) US-Ho1, Howland Forest, ME. (B) US-Me6 (Metolius Young Pine Burn), Metolius, OR. (C) US-Ton, Tonzi Ranch, *CA*. (D) Durham 11 W, Duke Forest, NC. (E) US-SRS (Santa Rita Savanna), Walnut Gulch, AZ. (F) US-Var (Vaira Ranch Ione), Tonzi Ranch, *CA*. (G) Stillwater 2 W, MOISST, OK. (H) Stillwater 5 WNW, MOISST, OK. Political state boundaries on the top of the U.S. are from (Homeland Infrastructure Foundation-Level Data (HIFLD), 2012). The soil texture triangle at the bottom (modified after (Sandrock and Afshari, 2016)) show indications on soil textures for every station (Table 1).

Table 1
Information on AirMOSS monitoring sites and *in situ* measuring stations.

AirMOSS site	Amount of dates (2013/2014/2015)	climate	*In situ* station	*In situ* network	NLCD Land Cover Class	Soil texture (Fig. 1)
Howland Forest, ME	21 (8/8/5)	Dfb	US-Ho1	AmeriFlux (Hollinger, 2021)	Evergreen Needleleaf Forests	Sandy Loam
Duke Forest, NC	22 (8/10/4)	Cfa	Durham 11 W	US-CRN	Pasture / Hay	Loam
Metolius, OR	21 (5/7/9)	Csb	US-Me6	AmeriFlux (Law, 2021)	Evergreen Needleleaf Forests	Sandy Loam/ Loamy Sand
MOISST, OK	19 (6/9/4)	Cfa	Stillwater 2 W Stillwater 5 WNW	US-CRN	Grassland / Herbaceous	Sandy Loam/ Loam Loam
Tonzi Ranch, CA	13 (3/6/4)	Csa	US-Ton US-Var	AmeriFlux (Ma et al., 2021) AmeriFlux (Ma et al., 2022)	Woody savanna Grassland	Loam
Walnut Gulch, AZ	15 (5/4/6)	BSk	US-SRS	AmeriFlux (Vivoni, 2022)	Woody Savanna / Shrubland	Sandy Loam

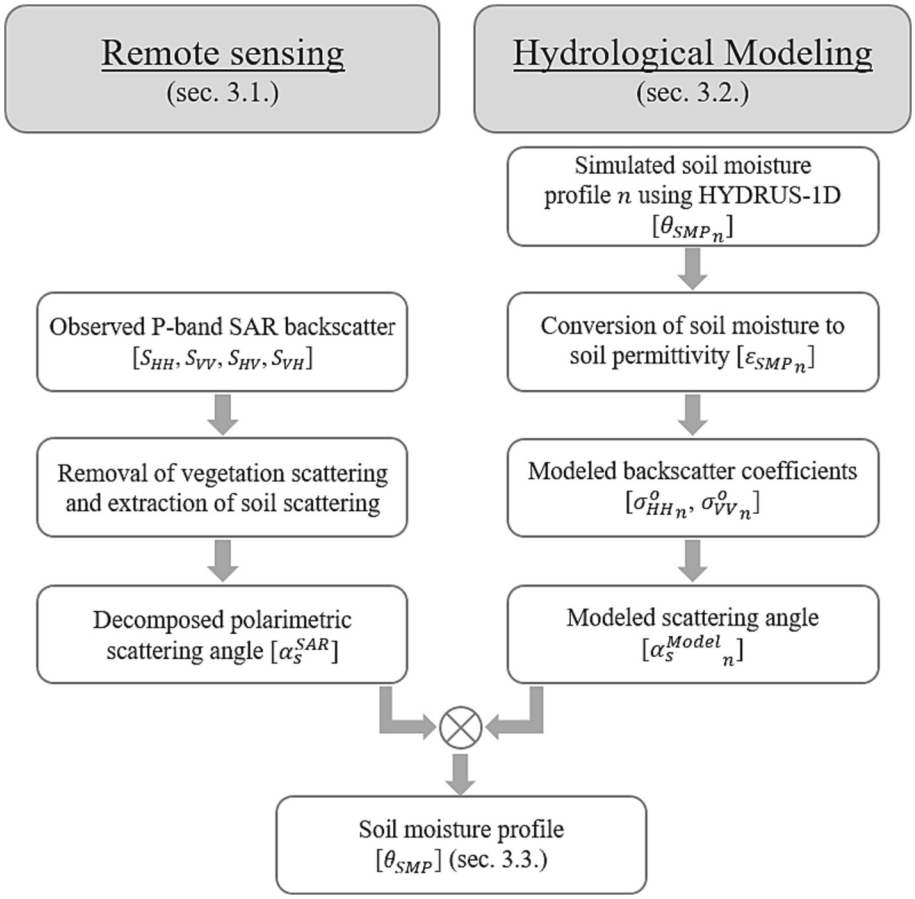

Fig. 2. Flow chart of the proposed joint technique combining remote sensing and soil (hydrological) modeling for estimation of soil moisture profiles.

$$\alpha_s^{SAR} = acos\left(\left(1 + 4^*\left(\frac{T_{12}^* - f_v V_{12}}{T_{11} - T_{22} - f_v V_{11} + f_v V_{22} - \sqrt{RT}}\right)^2\right)^{-\frac{1}{2}}\right), \quad (3)$$

with $RT = \left|T_{11}^2 + \left(T_{22} + f_v V_{11}\right)^2 + 4\left(T_{12} - f_v V_{12}\right)\left(T_{12}^* - f_v V_{12}\right) - 2T_{11}\left(T_{22} + f_v(V_{11} - V_{22})\right) - 2f_v\left(T_{22} + f_v V_{11}\right)V_{22} + f_v^2 V_{22}^2\right|$ (Fluhrer et al., 2022). For more details on the hybrid decomposition and removal of the vegetation component, the reader is referred to (Fluhrer et al., 2022; Jagdhuber et al., 2015).

In summary, for every observed SAR signal, one α_s^{SAR} is estimated from the soil scattering component after removing the dihedral and volume scattering components.

3.2. Modeled soil scattering angle based on coupled HYDRUS-1D and multi-layer SPM simulation

The HYDRUS-1D (Šimůnek et al., 2013) soil hydraulic model is used for simulating one-dimensional water flow with heat and vapor transport in variably saturated, homogeneous soils. The model numerically solves a modified version of the Richards equation by using the linear finite element method (Šimůnek et al., 2013):

$$\frac{\partial\theta}{\partial t} = \frac{\partial}{\partial x}\left[K\left(\frac{\partial h}{\partial x} + cos\alpha\right)\right] - S, \tag{4}$$

where θ is the volumetric water content [L^3/L^3], t is the time [T], x is the spatial coordinate [L], h as the soil matric potential [L], α giving the flow direction (= 0 [°] for vertical flow), S is the sink term [$L^3/L^3/T$] to account for root water uptake, and K is the unsaturated hydraulic conductivity function [L/T]. For simulations, the soil hydraulic properties, the soil water retention, $\theta(h)$, and soil hydraulic conductivity, $K(h)$, functions are given by the Van Genuchten-Mualem analytical model, which uses the statistical pore-size distribution model of (Mualem, 1976):

$$\theta(h) = \begin{cases} \theta_r + \dfrac{\theta_s - \theta_r}{[1 + |\alpha h|^n]^m} & h < 0 \\ \theta_s & h \geq 0 \end{cases}, \tag{5}$$

$$K(h) = K_s S_e^l \left[1 - \left(1 - S_e^{1/m}\right)^m\right]^2, \tag{6}$$

$$S_e = \frac{\theta - \theta_r}{\theta_s - \theta_r}, \tag{7}$$

where θ_r and θ_s are residual and saturated water contents [L^3/L^3], K_s is the saturated hydraulic conductivity [L/T], S_e is the effective saturation [−] given by (7), α is the inverse of the air-entry value (or bubbling pressure) [L^{-1}], n is the pore-size distribution index [−], $m = 1 - 1/n$, and l is the pore-connectivity parameter [−], which is assumed to be equal and set to 0.5 (Mualem, 1976). The Van Genuchten-Mualem parameters for every simulation are calculated in this study based on the pedotransfer function (PTF) of (Tóth et al., 2015) and input parameters from SoilGrids™ at 100 m spatial resolution (Nauman et al., 2017).

Additionally, to account for non-compensated water uptake by plant roots during simulations, the sink term S in (4) is calculated after the root-water uptake model from (Feddes et al., 1978), and the root water uptake stress response function after (Cai et al., 2018).

Within simulations, a non-uniform spatial variation of the potential extraction term is chosen by assuming a linearly decreasing water uptake distribution across the root zone (until assumed root depth) (Šimůnek et al., 2013). The assumed root depth, limiting the zone where root water uptake can occur within the vertical soil profile, was set at the soil depth of −1 m except for landcover class 'forests', where roots were assumed to expand across the entire soil profile. The heat transport parameters, namely the volume fraction of solid phase ($Q_n = 0.6\ [-]$) and organic matter ($Q_o = 0.0001\ [-]$), the longitudinal thermal dispersivity ($\lambda_L = 6\ [cm]$), and the heat capacities of solid phase ($C_n = 1.43327{*}10^{14}$), organic matter ($C_o = 1.8737{*}10^{14}$) and water ($C_w = 3.12035{*}10^{14}$) $[J/m^3/^\circ C]$, are fixed for all HYDRUS-1D simulations (Nakhaei and Šimůnek, 2014; Šimůnek et al., 2013). The parameters in the employed thermal conductivity function after (Chung and Horton, 1987), namely $b_1, b_2,$ and b_3 $[W/m/^\circ C]$, are depending on the respective sand, clay and silt fractions from SoilGrids™ (Nauman et al., 2017) for every SAR pixel.

The required meteorological and atmospheric input parameters at daily time scales, namely precipitation [mm], net solar radiation [MJ/m^2], sunshine hours [h], potential evaporation [mm], air temperature [°C], soil temperatures (for upper & lower boundary of the soil profile) [°C], average humidity [%], and wind speed [km/d], are taken from the *in situ* measuring stations (see Sec. 2.). Here, the number of sunshine hours per day was estimated from the measured incoming shortwave radiation. For that, the sum of hours per day, where the incoming shortwave radiation exceeded 120 $[W/m^2]$ (World Meteorological Organization, 2021) is calculated. The incoming shortwave radiation was taken from *in situ* measurements at every AmeriFlux station. For all other stations, namely Stillwater 2 W, Stillwater 5 WNW, and Durham 11 W (Table 1), the ERA5-land reanalysis product (Muñoz Sabater, 2019) is used.

Overall, the chosen simulation set-up in HYDRUS-1D assumes time-dependent atmospheric boundary conditions with variable runoff (Table 2) at the soil surface, and time-independent atmospheric boundary conditions with free drainage ($\partial h/\partial x = 0$) at the bottom of the profile. For heat transport, the first-type Dirichlet boundary condition at the soil surface (ponded infiltration) with zero gradient (continuous temperature profile) at the bottom was chosen. Further, no hysteresis in soil water retention and hydraulic conductivity is assumed, and initial water flow conditions are specified in terms of the soil matric potential (Šimůnek et al., 2013). For that, the absolute value of the minimum allowed soil matric potential on the soil surface is set to −100,000 [cm] (Cai et al., 2018), and the initial soil matric potential across the soil profile is kept variable (Table 2).

The HYDRUS-1D soil moisture profiles θ_{SMPn}, where n stands for one simulation within the ensemble, are always simulated on daily basis for one entire year with a three-month initialization period, in order to align initial conditions with given weather conditions. Lastly, a total of 101 simulation nodes, which were distributed non-linearly across the soil profile with decreasing density from the soil surface to the lower boundary of the determined soil column, have been defined. The input parameters that were kept flexible within simulations in order to minimize the amount of initial assumptions, and to calculate a variety of potentially occurring soil moisture profiles, are listed in Table 2. This means that for every *in situ* measuring station (Fig. 1, Table 1) and every AirMOSS acquisition year (2013 to 2015) 735 simulations were performed, respectively. All simulated HYDRUS-1D soil moisture profiles θ_{SMPn} are then converted to soil permittivity ε_{SMPn} according to the dielectric mixing model of (Mironov et al., 2009), and used as an ensemble input for backscatter simulations with the multi-layer SPM (Tabatabaeenejad and Moghaddam, 2006) (Fig. 2). Previous studies showed that at P-band, penetration depths between 10 cm to 30 cm soil depth are realistic for the investigated soil conditions in this study (Fluhrer et al., 2022; Konings et al., 2014). Hence, only the simulated soil moisture profile values of individual soil layers from the surface until a soil depth of 30 cm are considered for backscatter simulations in order to align with remotely sensed P-band SAR observations. For an assumed soil depth of 2 m during hydrological simulations, 36 individual soil moisture layers from the corresponding HYDRUS-1D simulation nodes between 0 and 30 cm are considered for backscatter simulations with the multi-layer SPM. For an assumed soil depth of 4 m, 24 individual soil moisture layers are considered (Table 3). This assumption on maximum soil depth of 30 cm for comparison is reasonable although, of course, the penetration depth of P-band SAR signals varies with different soil and vegetation cover conditions (*i.e.*, moisture, texture, density, *etc.*). It can be further improved in the future when sufficient information on penetration depths are available.

The first-order solution of the multi-layer SPM computes backscatter coefficients σ^o_{pp} from multiple subsurface layers by considering "multiple scattering processes between the boundaries" (Tabatabaeenejad and Moghaddam, 2006), suitable for analyzing P-band soil interactions. The required input parameters for modeling $\sigma^o_{pp}n$ and their respective values,

Table 2
Static values of input parameters for HYDRUS-1D soil moisture profile simulations.

HYDRUS-1D input parameter	Static values
Depth of soil profile [m]	2, 4
Maximum allowed soil matrix potential at the soil surface [cm]	0, −1, −5, −10
Initial soil matric potential across the soil profile [cm]	−250, −500, −1000, −2000, −4000, −8000, −16,000
Distribution of the initial soil matric potential across the soil profile [−]	Static, decreasing
Upper boundary condition for water flow [−]	Runoff, zero runoff (water can accumulate at the surface)

Table 3
Required input parameters for the multi-layer SPM to simulate $\sigma^o_{pp}n$, with the applied values in this study.

Parameter	Value
Frequency, f [MHz]	430
Number of layers, N [−]	36 (for soil profile depth of 2 m), 24 (for soil profile depth of 4 m)
Incidence angle in range, ϕ_i, and azimuth, φ_i [°]	ϕ_i from AirMOSS; $\varphi_i = 0$
Scattering angle in range ϕ_s, and azimuth, φ_s [°]	$\phi_s = \phi_i$; $\varphi_s = 180$ (backscattering)
z-coordinates of the respective boundary layers [cm]	Increasing from $\lambda/10$ (6.97) at the soil surface to $\lambda/2$ (34.86) at the profile bottom
Surface roughness parameters of each layer i [cm] (RMS height s, correlation length l)	s_i and l_i are dependent on a roughness indicator derived from TanDEM-X (Table 4)
Autocorrelation function, ACF [−]	Exponential
Permittivity ε_{SMPn} of each layer i [−]	From HYDRUS-1D simulated and converted soil permittivity profiles ε_{SMPn_i}

approximated for the acquisition scenario in this study, are listed in Table 3.

Due to the fact that no roughness information for any soil layers are available for the AirMOSS monitoring sites or *in situ* measuring stations, the DLR TanDEM-X DEM at 90 m resolution (Rizzoli et al., 2017) was used to get first-order roughness indicators for every SAR pixel. For that, the TanDEM-X elevations were converted with the GDAL DEM utility algorithm (GDAL/OGR contributors, 2021) in QGIS© (QGIS Development Team, 2021) to roughness values, giving the degree of irregularity of the surface, and scaled to the employed AirMOSS wavelength at P-band ($\lambda = 69.72$ [cm]) to account for the reduced impact of surface roughness at P-band than at X-band. Thus, depending on the estimated roughness indicator R_{TDX} (Table 4, left column) for every SAR pixel, typical surface roughness parameter sets for each layer i (Table 4, right column) are fixed as input for the multi-layer SPM to account for varying layer roughness (from smooth to rather rough).

The modeled $\sigma^o_{pp}n$ [−], for horizontal and vertical polarization, are then used to calculate for every simulation the model-based $\alpha_s^{Model}n$ after (Cloude, 2010), valid for $0 \leq \alpha_s \leq \frac{\pi}{2}$:

$$\alpha_s^{Model}n = tan^{-1}\left(\frac{\sigma^o_{HH}n - \sigma^o_{VV}n}{\sigma^o_{HH}n + \sigma^o_{VV}n}\right). \quad (8)$$

3.3. Joint technique of remote sensing and hydrological modeling for soil moisture profile estimation

From remote sensing, one α_s^{SAR} value for every resolution cell and recording date can be estimated (see Sec. 3.1.). From soil hydrological modeling, an ensemble of $\alpha_s^{Model}n$ for n simulations can be calculated for every resolution cell and recording date based on varying initial settings (see Sec. 3.2.). In order to determine the most suited soil moisture profile for every resolution cell and recording date, the observed remote sensing information is compared with all hydrological modeling outputs. In detail, the actual observed α_s^{SAR} from measured SAR observations is used to select the most suited soil moisture profile from hydrological modeling. The smallest absolute differences between α_s^{SAR} and all $\alpha_s^{Model}n$ is then used to estimate the final soil moisture profile:

$$\theta_{SMP} = argmin\left(\left|\alpha_s^{SAR} - \alpha_s^{Model}n\right|\right) \quad (9)$$

In Fig. 3A, the ensemble of simulated soil moisture profiles θ_{SMPn}, based on HYDRUS-1D, are displayed at station US-SRS, Walnut Gulch, AZ, on the 12th of July in 2014. It can be seen that the different assumptions on initial model conditions lead to various soil moisture profile shapes. For every simulated soil moisture profile θ_{SMPn}, the procedure described in Sec. 3.2. is applied to obtain the model-based $\alpha_s^{Model}n$. Finally, the best fit between α_s^{SAR} and all $\alpha_s^{Model}n$ is estimated (Fig. 3B). A sensitivity study was conducted to analyze the estimation procedure regarding potential multiple solutions and uncertainties of the best fit. It was found that the method estimates the global minimum (always only one single best fit) with 2nd best and higher best fits deviating at least 1.75% from the best one. In the end, the comparison of the SAR-extracted soil information is indicative for selecting the appropriate soil moisture profile. For one, the estimated θ_{SMP} profile fits best to *in situ* measurements (green stars in Fig. 3B). Second, although the upper soil moisture conditions cannot be confirmed by *in situ* observations, the decrease in soil moisture values between 0 cm and 3.8 cm soil depth match the apparent soil and meteorological conditions, as described in detail in Sec. 4.

Table 4
Surface roughness parameter sets for each layer i (RMS height s, correlation length l; step size equals number of layers) within the multi-layer SPM based on TanDEM-X derived roughness indicators R_{TDX}.

Roughness Indicator From Tandem-X [M]	Input Roughness Parameters [CM]
$R_{TDX} < 5$	$s_i = 0.5 - 0$; $l_i = 30 - 60$
$5 \leq R_{TDX} < 10$	$s_i = 1.5 - 0.75$; $l_i = 25 - 50$
$10 \leq R_{TDX} < 15$	$s_i = 2 - 1$; $l_i = 20 - 40$
$R_{TDX} \geq 15$	$s_i = 3 - 1.5$; $l_i = 15 - 30$

4. Results

In this study, the Pearson's coefficient of determination R^2, the unbiased root mean square error (*ubRMSE*), giving the error between curves without the mean bias (Maity, 2022), and the Fréchet distance F (Fréchet, 1906), representing the curve shape similarity, are employed for statistical analyses. F provides the similarity of curves taking into account not only absolute values but also the ordering of points along the investigated curves (Eiter and Mannila, 1994). Further, since auxiliary products are only available at discrete soil depths (*i.e.* symbols in Fig. 4), a polynomial function of 2nd order is applied to combine these values in order to estimate the approximate profile shapes for comparison. Although it is known that polynomials are physically unrealistic and can only give an approximate of the vertical soil moisture variability (see Sec. 1.), it is used in this study to be able to compare not only results at two to three discrete measuring depths but also across the entire soil column to evaluate the shape of the estimated soil moisture profiles.

In total, three types of typical soil moisture profiles could be observed within all estimated results, depending on prior precipitation events and soil conditions. As shown in Fig. 4A, a typical drying profile with increasing soil moisture at increasing soil depths was estimated when, at the respective station, no precipitation occurred at least seven days prior to the recording date. The soil dries at different rates, according to the soil type and texture, from the soil surface towards deeper soil layers. In contrast, a typical wetting profile could be observed when, at this station, precipitation occurred some days before the recording date (Fig. 4B). The soil moisture profile decreases with increasing soil depth since the water infiltrates from the soil surface downwards to the deeper soil layers. The depth of the inflection point varies depending on the infiltration rate and elapsed time since the rain event. In the presented example, the decrease in soil moisture values at the top (from 0 cm to −4.5 cm) of the soil is rather rapid and the profile below is rather dry at ~18 vol% because of the local conditions around the station US-SRS. At this station in Arizona an (hyper-)arid climate with warm summers led to predominantly shrublands on top of sandy loam soils (62% sand fraction, ~19% silt and clay fractions) (Fig. 1, Sec. 2.). This means, precipitation is less frequent and water can infiltrate rather quickly into the uppermost soil layers. At other stations with different soil and landcover conditions, *e.g.* at the forest station US-Ho1, the decrease in soil moisture values was less rapid and more continuous.

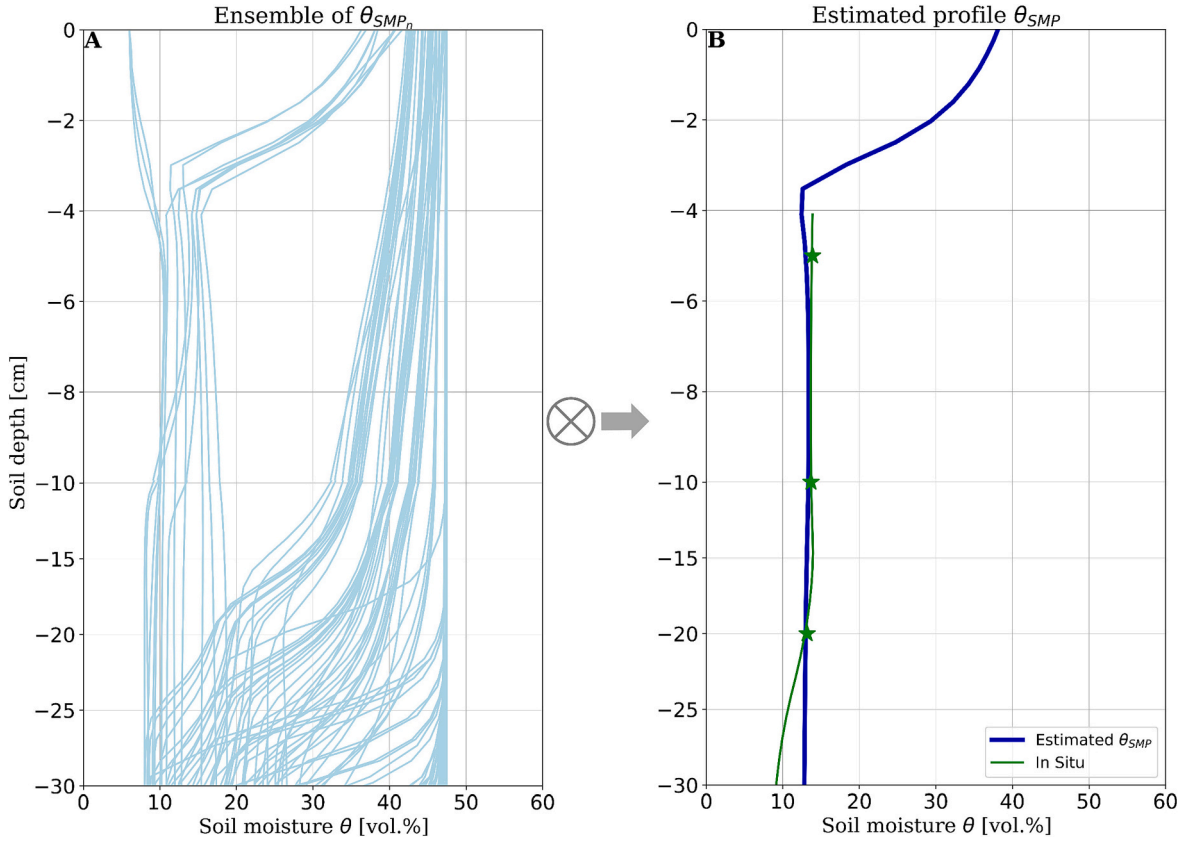

Fig. 3. Visualization of the estimation procedure to determine the best fitting soil moisture profile $\boldsymbol{\theta_{SMP}}$ from all simulated $\boldsymbol{\theta_{SMP_n}}$ by comparing SAR observations with soil modeling. (A) Ensemble of simulated $\boldsymbol{\theta_{SMP_n}}$ from HYDRUS-1D based on varying initial conditions (Table 2, Sec. 3.2.) at station US-SRS, Walnut Gulch, AZ, on the 12th of July 2014. (B) Estimated soil moisture profile $\boldsymbol{\theta_{SMP}}$ at station US-SRS, Walnut Gulch, AZ, on the 12th of July 2014, in comparison to *in situ* observations from the same day.

Lastly, saturated profiles at higher moisture values with almost no variation across the vertical soil column were estimated after heavy precipitation events prior to the recording date (Fig. 4C). Unfortunately, no soil moisture comparison data could be found for soil depths between 0 to −5 cm to confirm the upper conditions. However, it can be seen that all three estimated profiles from the proposed method (SAR with hydrological modeling) fit best to the *in situ* measurements with overall highest correlation coefficients, lowest *ubRMSE* and smallest Fréchet distances, hence, highest similarity not only in absolute values but also in profile shape along the vertical soil column (Table 5, upper rows). Further, statistics are overall better between estimated profiles and *in situ* measurements compared to statistics between *in situ* measurements and auxiliary products (ERA5-land, AirMOSS L4) (Table 5, lower rows). While significantly high $R^2 \geq 0.93$ are found between estimated soil moisture profiles and *in situ* measured profiles, overall lower $R^2 \leq 0.64$ are found between *in situ* measurements and auxiliary products. Correspondingly, overall higher *ubRMSE* and *F* are found, except for the wetting profile at station US-SRS (Fig. 4b), where the same *ubRMSE* of 1 vol% for all comparisons and slightly better *F* between *in situ* measurements and the AirMOSS L4 product are found (Table 5).

In this study, soil moisture profiles are only shown from the soil surface until a depth of 30 cm, since this part of the simulated soil moisture profiles are used for comparison with P-band SAR observations (see Sec. 3.2.). In the following, soil moisture profiles are presented first for all measuring stations (see Sec. 4.1.), and then detailed analyzes are performed at two selected stations (see Sec. 4.2.).

4.1. Soil moisture profile results for all measuring stations

In Figs. 5 and 6, estimated soil moisture values between 0 cm to −30 cm soil depth for all available AirMOSS dates are compared with corresponding auxiliary profiles. Here, individual plots of kernel density estimates show the conditional distribution of values with indications on the density of values (the darker the color, the higher the amount of values) and the fitted linear regression (solid line). First, the measuring stations with landcover types forest (Fig. 5, 1st and 2nd row), woody savanna (Fig. 5, 3rd row) or shrublands (Fig. 5, 4th row) are displayed (Fig. 1, Sec. 2.). Noticeable is the overestimation of soil moisture values from all three auxiliary products at the two forest stations, with more significant overestimation at the more homogeneously vegetated station, US-Ho1, covered by dense forests (Fig. 5, 1st row). At the less densely vegetated forest station, US-Me6 (Fig. 1, Sec. 2.), estimated soil moisture values range between 10 vol% and 38 vol%, while *in situ* measurements only indicate values between 2 vol% and 22 vol%. Here, the rather dry *in situ* measured values (highest density at 6.9 vol%) are overestimated with the proposed approach, similar to the ERA5-land product. In contrast, good agreement between estimated values and the AirMOSS L4 product can be observed, with highest density of values around the 1:1 line (Fig. 5, 2nd row). Further, at the woody savanna station, US-Ton, the highest density of values is located close to the 1:1 line, with a slight overestimation of rather dry *in situ* measurements and ERA5-land values. Noticeable at this station are the two additional, very dominant accumulations of values.

One at low estimated soil moisture values around 18 vol% and high *in situ* measurements around 37 vol%. And one around the 1:1 line between 35 vol% and 40 vol%. This means, correlations between estimated and *in situ* measured soil moisture values increase, when *in situ* measured values increase, but with some exceptions, where higher field measurements are in turn underestimated with the proposed approach (Fig. 5, 3rd row). Unfortunately, no AirMOSS L4 soil moisture profiles

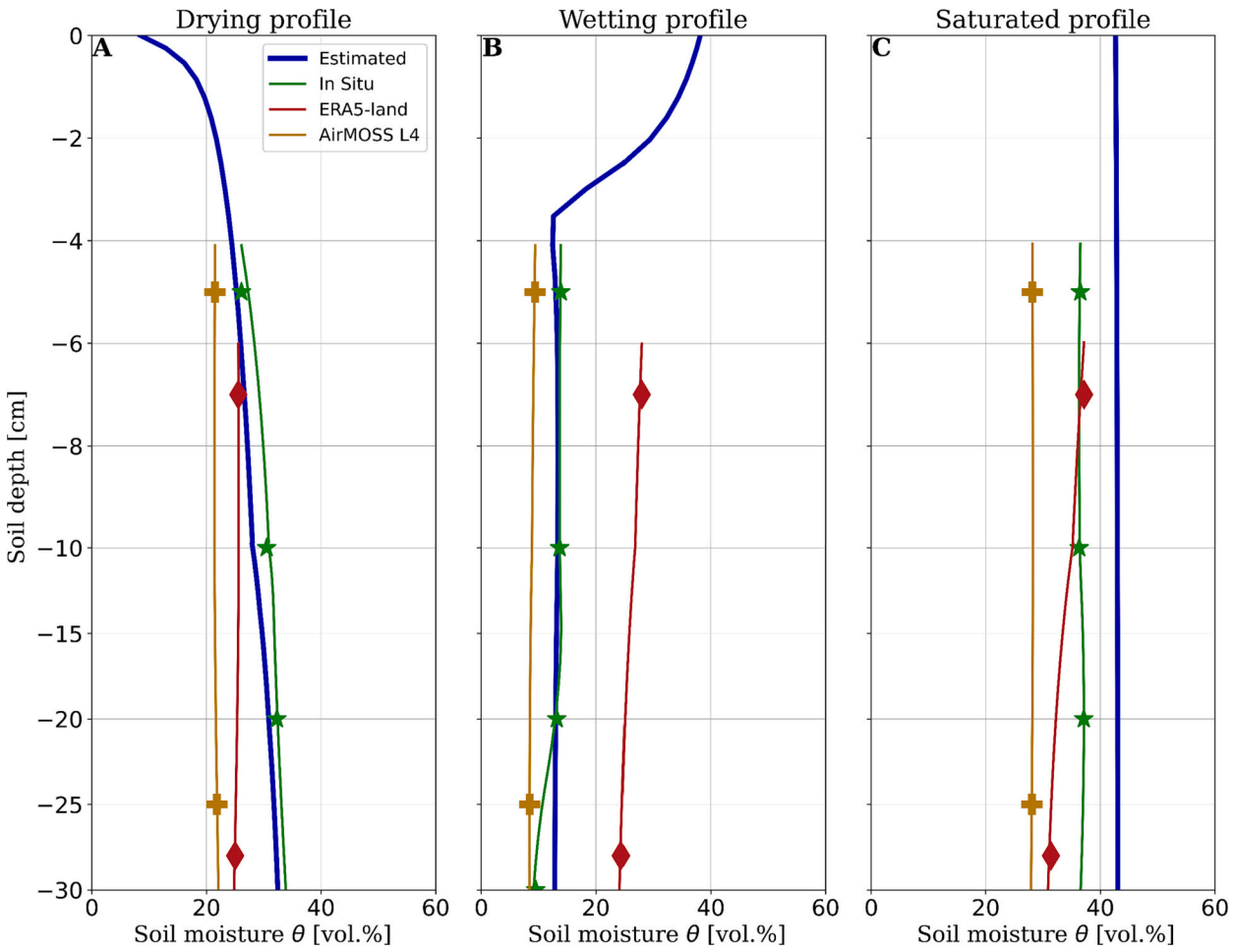

Fig. 4. Typical profile shapes of estimated soil moisture profiles based on the proposed approach in comparison with auxiliary soil moistures products of the same day. (A) Drying profile on the 21st of October 2014 at station Stillwater 2 W, MOISST, OK (no precipitation). (B) Wetting profile on the 12th of July 2014 at station US-SRS, Walnut Gulch, AZ (51.6 mm of precipitation in the week before the recording date). (C) Saturated profile on the 17th of June 2013 at station Stillwater 5 WNW, MOISST, OK (in total 57.6 mm of precipitation two days before the recording date). The y-axis is stretched between 0 cm and − 10 cm to emphasize the most dynamic part of the soil moisture profile.

Table 5
Statistical measures between estimated (upper rows) or *in situ* measured (lower rows) soil moisture profiles and auxiliary profiles displayed in Fig. 4.

Statistical measure	Drying profile			Wetting profile			Saturated profile		
	Estimated *vs.*			**Estimated *vs.***			**Estimated *vs.***		
	In Situ	**ERA5**	**AirMOSS L4**	***In Situ***	**ERA5**	**AirMOSS L4**	***In Situ***	**ERA5**	**AirMOSS L4**
R^2 [−]	0.95	0.71	0.61	0.93	0.64	0.57	0.95	0.58	0.22
ubRMSE [vol%]	0.3	1.2	1.6	1	1.1	2.1	0.3	2	0.1
F [−]	0.02	0.08	0.1	0.08	0.1	0.09	0.07	0.1	0.2
	In situ vs.			***In situ vs.***			***In situ vs.***		
	ERA5		**AirMOSS L4**	**ERA5**		**AirMOSS L4**	**ERA5**		**AirMOSS L4**
R^2 [−]	0.61		0.45	0.59		0.37	0.64		0.13
ubRMSE [vol%]	2		2	1		1	2		0
F [−]	0.09		0.12	0.15		0.05	0.06		0.09

are available at this station and two others (Fig. 6). Lastly, at the desert station US-SRS in Arizona, similar patterns as describe before can be seen. While estimated soil moisture values range between 10 vol% and 45 vol%, *in situ* measurements range between 10 vol% and 20 vol%. Again, the estimated values overestimate the rather dry *in situ* measurements (highest density at 8.8 vol%), similar as to the AirMOSS L4 product, which, at this station, shows the smallest value range of all (between 8.4 vol% to 17.3 vol%). Only the ERA5-land product achieves similar value ranges compared to the estimated values, with the highest density of values deviating approximately 6 vol% from the perfect fit (1:1 line) (Fig. 5, 4th row).

When analyzing all results at the pasture station Durham 11 W (Fig. 6, 3rd row), most estimated and *in situ* measured soil moisture values are close to the 1:1 line, with a tendency to an overestimation of

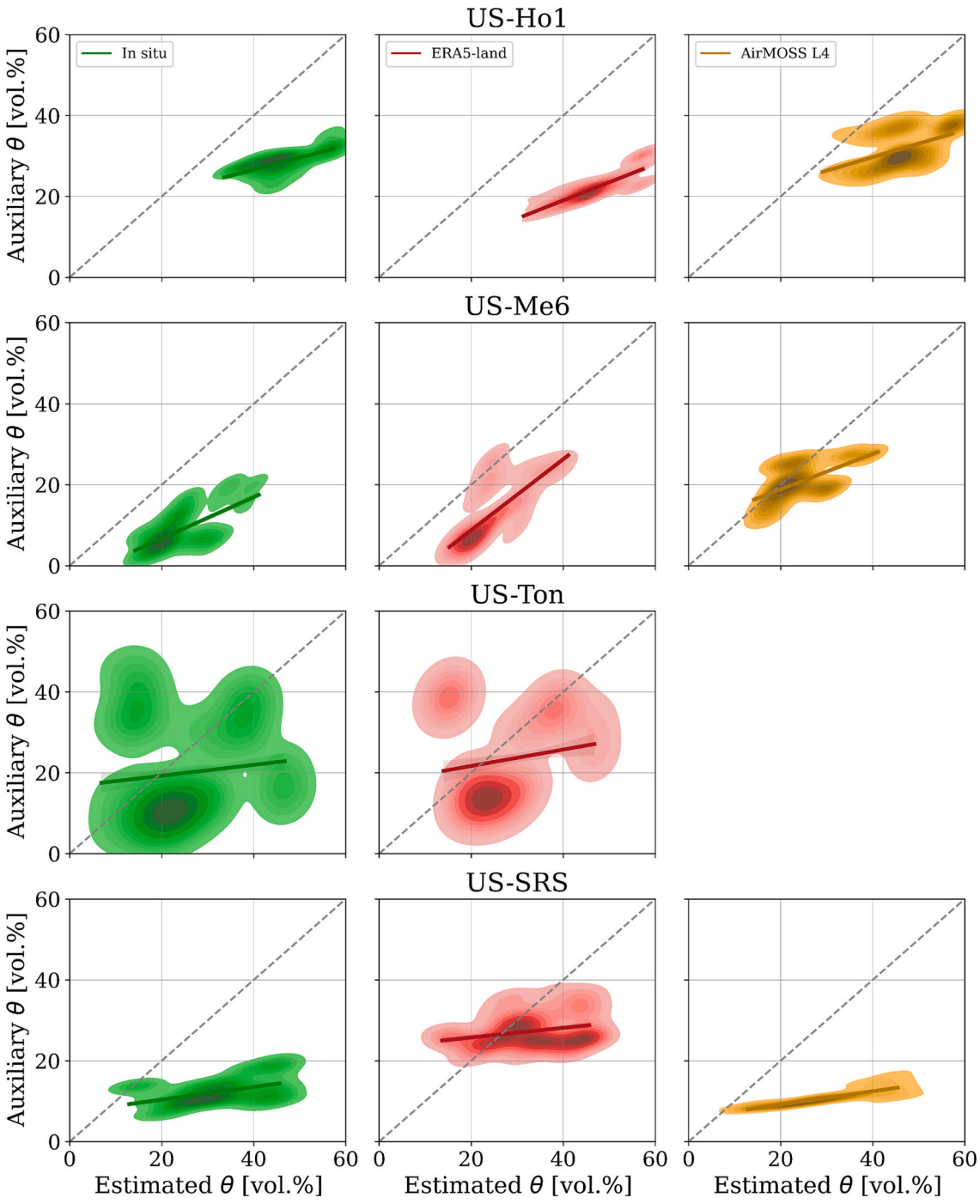

Fig. 5. Comparison of estimated soil moisture values for all layers from soil depths between 0 cm to −30 cm, with auxiliary soil moisture products of the corresponding same recording day (including all AirMOSS overflight dates between 2013 and 2015). 1st row: US-Ho1, Howland Forest, ME. 2nd row: US-Me6, Metolius, OR. 3rd row: US-Ton, Tonzi Ranch, *CA*. 4th row: US-SRS, Walnut Gulch, AZ.

estimated moisture values for decreasing *in situ* measurements. In contrast, the comparison between estimated values and the ERA5-land product shows a slight underestimation, as most ERA5-land soil moisture values are in the range of 38 vol% to 42 vol%, whereas most estimated values range between 22 vol% and 40 vol% (Fig. 6, 3rd row). Lastly, analyzing the results at the two grassland and one shrubland station (Fig. 6, 1st, 2nd and 4th row) similar results as those for the previously described stations can be seen, except for the station Stillwater 2 W in Oklahoma (Fig. 6, 2nd row). Here, estimated and *in situ* measured soil moisture values are closest to the 1:1 line with lowest deviations, confirmed by the overall highest correlation of all stations with a R^2 of 0.92 (Table 6). Similar to the first station at the AirMOSS site Tonzi Ranch, US-Ton (Fig. 5, 3rd row), the second shrubland station US-Var also shows a large variety in soil moisture values with several accumulation spots (Fig. 6, 4th row). The highest density of estimated and *in situ* measured values, however, are located at the 1:1 line, which explain the clearly higher R^2 of 0.81 compared to the R^2 of just 0.59 at US-Ton.

Further, compared to all other stations, these two stations in California show the overall highest *ubRMSE* of 2.9 vol% and 3.7 vol%, respectively (Table 6). In Table 6, the statistical measures between estimated soil moisture profiles and the corresponding auxiliary products (upper rows) as well as between *in situ* measurements and ERA5-

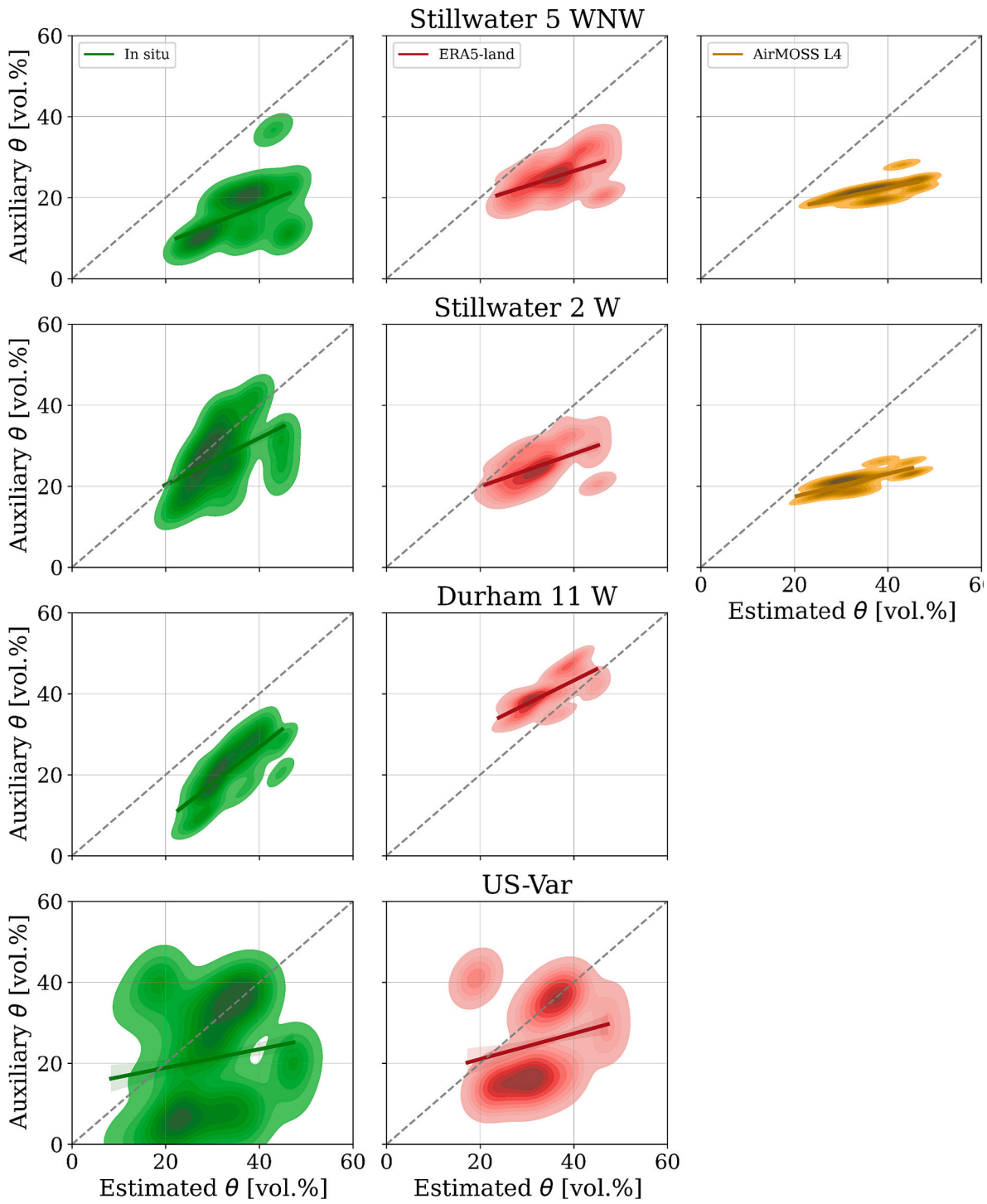

Fig. 6. Comparison of estimated soil moisture values for all layers from soil depths between 0 cm to −30 cm, with auxiliary soil moisture products of the corresponding same recording day (including all AirMOSS overflight dates between 2013 and 2015). 1st row: Stillwater 5 WNW, MOISST, OK. 2nd row: Stillwater 2 W, MOISST, OK. 3rd row: Durham 11 W, Duke Forest, NC. 4th row: US-Var, Tonzi Ranch, *CA*.

land or AirMOSS L4 products (lower rows) are displayed. In general, when comparing the estimated soil moisture profiles with all auxiliary products, the R^2 varies between 0.32 and 0.94, the *ubRMSE* ranges from 0.7 vol% to 3.7 vol%, and the F varies between 0.07 and 0.26 [−]. In detail, the overall highest R^2, lowest *ubRMSE* and smallest F are found between estimated soil moisture profiles and the ERA5-land product. This simply means, that the proposed method and the reanalysis method for soil moisture estimation agree well for soil depths between −7 cm and − 30 cm (ERA5-land values are available for −7 cm and − 28 cm), where changes in the soil moisture profile are less prominent (see Sec. 1).

With focus on the *in situ* observations, R^2 between 0.48 and 0.92 are reached in comparison with the estimated soil moisture profiles. Further, F varies between 0.1 and 0.23 [−], overall confirming the high similarity in profile shapes along the vertical soil column, since F varies in total between 0 (identical lines) and 0.4 (no similarity between lines) in this study. In absolute values (*ubRMSE* varying between 1.4 vol% and 3.7 vol%) the estimated results deviate from the *in situ* measured soil

Table 6
Statistical measures between estimated (upper rows) or *in situ* measured (lower rows) soil moisture profiles from 0 cm to −30 cm soil depth and auxiliary products at all measuring stations and all available AirMOSS dates. R^2 gives Pearson's coefficient of determination, *ubRMSE* the unbiased error, and *F* the Fréchet distance.

Statistical measure	Estimated results *vs.*	Station							
		US-Ho1	US-Me6	US-Ton	US-SRS	Durham 11 W	Stillwater 5 WNW	Stillwater 2 W	US-Var
R^2 [−]	*In situ*	0.52	0.71	0.59	0.49	0.48	0.59	0.92	0.81
	ERA5-land	0.78	0.87	0.79	0.9	0.76	0.89	0.94	0.88
	AirMOSS L4	0.32	0.49		0.81		0.76	0.86	
ubRMSE [vol%]	*In situ*	1.84	1.38	3.69	2.47	1.86	1.61	2.89	2.92
	ERA5-land	1.05	0.95	0.77	1.47	1.41	1.05	1.32	1.46
	AirMOSS L4	1.67	1.65		1.88		0.71	1.29	
F [−]	*In situ*	0.22	0.17	0.19	0.23	0.13	0.22	0.1	0.19
	ERA5-land	0.26	0.13	0.12	0.1	0.09	0.13	0.1	0.13
	AirMOSS L4	0.17	0.07		0.21		0.17	0.14	
	In situ results vs.								
R^2 [−]	ERA5-land	0.53	0.69	0.89	0.43	0.53	0.66	0.9	0.56
	AirMOSS L4	0.62	0.41		0.52		0.54	0.79	
ubRMSE [vol%]	ERA5-land	1.32	1.48	0.77	1.4	2.45	1.06	3.37	1.38
	AirMOSS L4	1.2	1.9		1.13		1.5	3.88	
F [−]	ERA5-land	0.08	0.06	0.05	0.17	0.21	0.11	0.1	0.07
	AirMOSS L4	0.07	0.16		0.02		0.08	0.13	

moisture profiles. However, the overall profile shapes are very well captured with this approach. The reasons why the *in situ* measurements fit a bit less to the estimated profile results (compared to the ERA5-land results) are, on the one hand, because they are constantly really low. For example, at the forest station US-Me6 in Oregon no *in situ* measured soil moisture value exceeds 24 vol%, and in average a soil moisture value of just 9.5 vol% was observed. On the other hand, because they vary quite much along the profile, indicating a high change in soil moistures within only a few cm of soil depth. Here, the highest change within *in situ* measured soil moisture values are observed at the forest station US-Me6 with a change of 13.2 vol% between −10 cm (7.1 vol%) and − 30 cm (20.3 vol%) soil depth. Further, in average soil moisture differences of 6.3 vol% within just 20 cm soil depth (between −10 cm and − 30 cm) are measured at this station across all dates.

Lastly, comparing estimated soil moisture profiles with the AirMOSS L4 product, the lowest R^2 of all stations and products can be found at the forest station US-Ho1. Here, the AirMOSS L4 product almost always significantly underestimates the estimated profiles. This is exacerbated by the fact, that the AirMOSS L4 products almost always leads to more or less uniform soil moisture profiles, showing no changes is soil moisture values across the vertical soil column, as displayed in the three examples of Fig. 4.

For comparison, additional statistics between *in situ* measurements and the two auxiliary soil moisture products are conducted. At some stations, the statistics between *in situ* measurements and the ERA5-land or AirMOSS L4 product are better (*i.e.*, US-Ho1), but at others not (*i.e.*, Stillwater 2 W). The slightly better performance of the two auxiliary products at the homogeneous forest station US-Ho1, with higher R^2 and lower *ubRMSE* and *F*, is the consequence of the already described overestimation of estimated values compared to the *in situ* measurements (Fig. 5, 1st row). Overall however, no clear pattern can be found when comparing the performance of statistics at all stations, dates and depths.

4.2. Detailed analyses at the two measuring stations US-Ho1 and Stillwater 2 W

In this section, results for estimated soil moisture profiles are

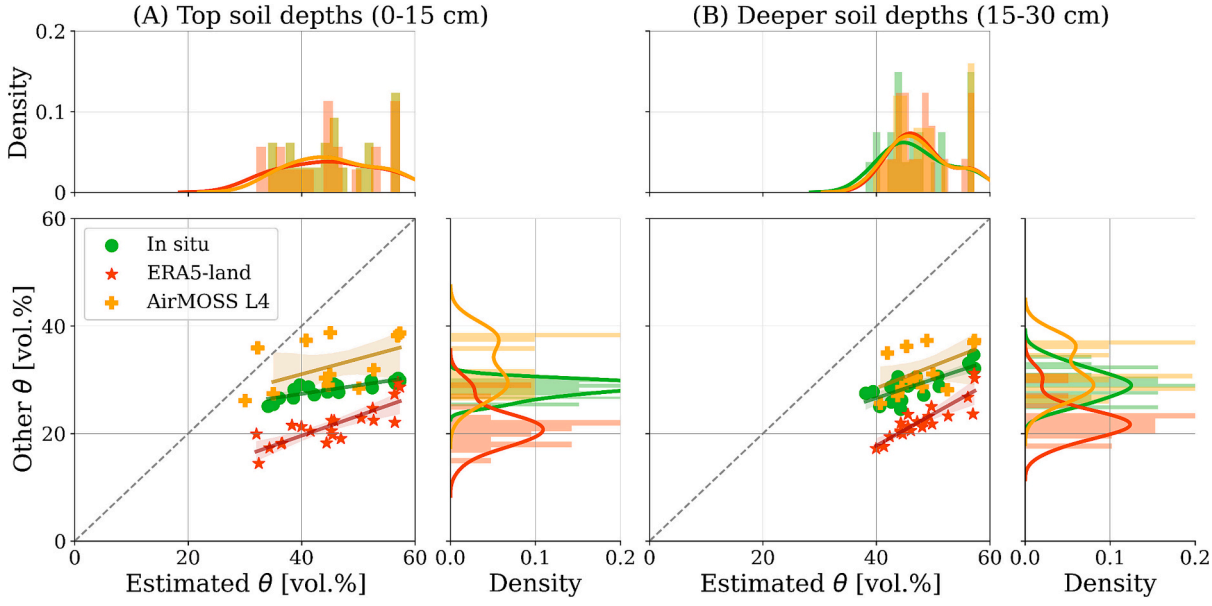

Fig. 7. Comparison of estimated soil moisture values between 2013 and 2015 at specific depths with auxiliary soil moistures products at monitoring stations US-Ho1, Howland Forest, ME. (A) Top soil depths (0–15 cm). (B) Deeper soil depths (15–30 cm).

analyzed in more detail at two selected stations, the most homogeneous forest station US-Ho1, and the grassland station Stillwater 2 W (Fig. 1 & Table 1, Sec. 2.).

In Figs. 7 and 8, auxiliary soil moisture values at actual measuring depths are compared to the respective estimated soil moisture values. The measuring depths are hereby divided into two groups, top soil and deeper soil depths. This way, different layers of the soil moisture profiles can be analyzed in addition. *In situ* measurements at station US-Ho1 are available from the AmeriFLX network at −10 cm and − 20 cm, and at station Stillwater 2 W from the US-CRN network at −5 cm, −10 cm, and − 20 cm soil depth (see Sec. 2.). ERA5-land soil moisture values are available for soil depths at −7 cm and − 28 cm, while the AirMOSS L4 product provides values for the integrals between 0 and 10 cm and 10–40 cm. For the latter, the average depths at −5 cm and − 25 cm were considered for comparison. This simplification does not affect the analyzes since the AirMOSS L4 product, as shown before, almost always results in more or less uniform soil moisture profiles (Fig. 4).

At the forest station, US-Ho1, estimated soil moisture values at deeper soil depths (Fig. 7B) overestimate auxiliary soil moisture products considerably more than estimated values at top soil depths (Fig. 7A). Here, results are almost always beyond 40 vol%, while auxiliary values mostly range between 20 vol% to 40 vol%. This is also supported by statistical measures since the R^2 between estimates and *in situ* measurements decreases from 0.68 for top soil depths to 0.61 for deeper soil depths. In contrast, the R^2 between estimates and ERA5-land or AirMOSS L4 values increases from 0.67 to 0.77 or 0.2 to 0.26 from top soil to deeper soil depths due to less variations within results. This is confirmed by the improved *ubRMSE* from 5.5 vol% to 2.7 vol% for ERA5-land, and from 6.5 vol% to 4.6 vol% for AirMOSS L4. Moreover, the probability density plots (PDFs) next to the scatterplots show that at this station the auxiliary products are not overlapping and deviate from another. The value ranges of the ERA5-land and AirMOSS L4 products hardly overlap with the *in situ* measured values at top soil depths (Fig. 7A). Only at deeper soil depths, the value ranges of the AirMOSS L4 product and the *in situ* measured ones converge (Fig. 7B).

In contrast, at measuring station Stillwater 2 W in Oklahoma, estimated values are overall closer to auxiliary values with always higher correlations for top soil values (Fig. 8). Here, the R^2 between estimates and *in situ* measurements decreases from 0.41 for top soil depths to 0.08 for deeper soil depths. Similar, the R^2 decreases from 0.43 for top soil depths to 0.15 for deeper soil depths between estimates and ERA5-land values, as well as from 0.58 for top soil depths to 0.55 for deeper soil depths between estimates and AirMOSS L4 values. Further, auxiliary products at this station are more overlapping since the value ranges clearly overlap with another as shown in the PDFs of Fig. 8. Only for deeper soil depths, the *in situ* measurements reach considerably higher values compared to the ERA5-land and AirMOSS L4 product (Fig. 8B).

5. Discussion

In this study, soil moisture profile shapes for drying, wetting and saturated soil conditions are estimated (Fig. 4, Sec. 4.). In order to obtain continuous soil moisture profiles, the decomposed SAR remote sensing scattering component of the soil is compared to soil hydrological simulations with HYDRUS-1D, converted to a soil scattering component by the multi-layer SPM scattering model. The comparison of the soil components is performed on the level of the polarimetric soil scattering angle α_s (see Sec. 3.). In previous studies, soil moisture retrieval approaches are mainly conducted on the level of backscattering, *e.g.* (Huang et al., 2021; Kim and Liao, 2021; Konings et al., 2014). This way, remotely sensed backscatter coefficient can be used without the preceding application of a decomposition technique. However, since SAR backscatter coefficients contain scattering mechanisms of all targets within the SAR footprint (soil, vegetation, and the combination of both), this circumstance in turn complicates the modeling of backscattering. In order to compare SAR backscatter coefficients with modeled backscatters, the combined soil and vegetation scattering has to be modeled first. Fortunately, in this study, only soil scattering has to be modeled since the decomposed soil scattering component of the total SAR signal is used for comparison. Certainly, the application of a decomposition method to extract the soil scattering from the SAR signal is not that simple and requires certain preconditions, like fully polarimetric SAR observations. However, as emphasized in Sec. 3., the comparison on the level of α_s instead of backscatters has several advantages (*e.g.*, no modeling of complex vegetation). Nevertheless, one of the main restrictions of this approach, for sure, is the correct removal of the vegetation component from the SAR signal. As outlined in many previous studies, *e.g.* (He et al., 2016; Jagdhuber, 2012; Sato et al., 2012; van Zyl et al., 2011), decomposition techniques tend to overestimate the vegetation scattering component, which leads to (physically impossible) negative

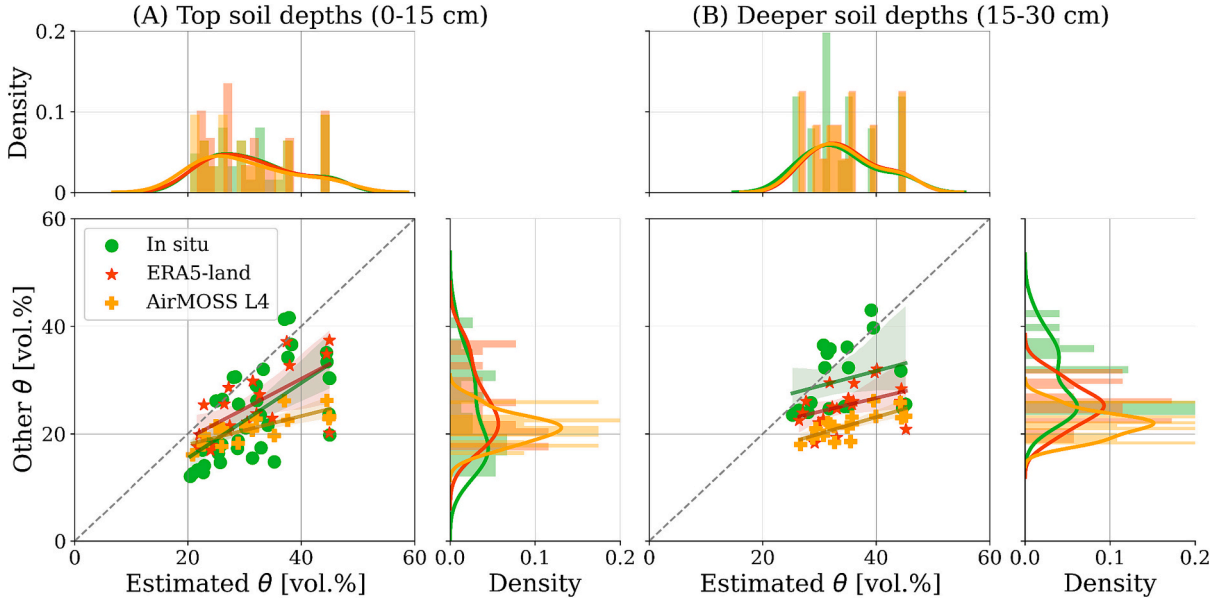

Fig. 8. Comparison of estimated soil moisture values between 2013 and 2015 at specific depths with auxiliary soil moistures products at monitoring station Stillwater 2 W, MOISST, OK. (A) Top soil depths (0–15 cm). (B) Deeper soil depths (15–30 cm).

decomposed powers (Fluhrer et al., 2022). Similar to the study of (Fluhrer et al., 2022), this problem is solved here by allowing multiple vegetation representations (see Sec. 3.1.), instead of fixing them to, for instance, 'a cloud of randomly oriented dipoles' (Alemohammad et al., 2018). This potential overestimation of vegetation during the decomposition is considered as one of the reasons why at the dense forest station US-Ho1 an overestimation of *in situ* measurements occurs (Fig. 5, Sec. 4.1.). Here, an improved removal of the vegetation scattering component by, for instance, including machine learning, may even decrease the overestimation of soil moisture profile estimates as indicated by (Fluhrer et al., 2022). Another reason could be that, as shown from (Fluhrer et al., 2022), in strongly vertically oriented vegetated areas, like the boreal forest at US-Ho1, the dihedral scattering mechanism is dominant in the total SAR signal. However, in this study the soil scattering mechanism is considered within the retrieval, which hence, may not be representative enough under dense and strongly oriented forests. This explanation is strengthend by the fact that at the other, less vegetated stations overall higher correlations with less pronounced overestimation are determined. Further, the highest correlation between estimates, based on this approach, and *in situ* measurements are found at the grassland station Stillwater 2 W (Sec. 4.). Also other studies, *e.g.* (Lucas et al., 2004; Moghaddam and Saatchi, 1995), outlined 'that at P-band the ground and trunks contribute with more relevance to the SAR signal than the branches and leaves'(Fluhrer et al., 2022), leading to dominant dihedral scattering components. However, using the dihedral scattering components instead of the soil scattering component is not an option for the proposed method. The main reason is that the estimation of soil moisture profiles with depth requires SAR observations from a comparable integral of the soil surface until the main scattering center within the soil. Here, the actual sensitivity depth of the soil part within the dihedral scattering component has to be further analyzed beforehand.

One of the advantages of the proposed approach is that profiles can be estimated more continuously along their vertical gradient and without the assumptions of empirical mathematical functions (*i.e.* polynomials of certain degree), *e.g.* (Etminan et al., 2020; Sadeghi et al., 2016; Tabatabaeenejad et al., 2015). As shown in the results section, no auxiliary soil moisture values could be found for continuous validation with soil depth since *in situ* measurements are done once between 0 and 5 cm soil depth or lower. However, this circumstance in turn emphasizes the need for the proposed approach (or similar ones), since it is able to provide continuous soil moisture profiles also for near-surface soil depths, and hence, capture this most variable uppermost part of soil moisture profiles more closely and reliable. This is of utmost importance since, as outlined in section one, near-surface soil moisture responds faster to environmenal changes because of, *e.g.*, precipitation or evaporation, and is more variable compared to subsurface soil moisture. Further, the approach provides the advantage that simulations are not restricted to a single model set-up. Admittingly, the simulation of an ensemble of soil moisture profiles for varying model set-ups and potentially for different locations is computationally expensive. However, the practicality of the proposed approach benefits from the circumstance, that the computationally highly expensive hydrological model simulations can be done independently from processing of the remote sensing observations, *e.g.*, on HPC (high performance computing) clusters. Further, the model simulations only need to be done once for the desired time series and can then be endlessly analyzed for different remote sensing observations (in case the model set-up fits the remote sensing set-up). Hence, the final comparison of hydrological model outputs and remote sensing observations for soil moisture profile estimation is less computationally expensive and can further be done for every SAR observation date separately, enabling, *e.g.*, parallel processing. This allows soil moisture profile simulations to be less prone to errors since variable assumptions on critical input parameters, such as the initial pressure head or the upper soil condition, reduce the potential for erroneous model runs. Here, the decomposed SAR observations, after the removal of the vegetation and double-bounce scattering components, is employed to provide the most realistic simulation compared to actual observations and hence, the most suited initial model set-up. In a follow-on study, this approach could be even used to analyze and improve initial model conditions and their susceptibility to errors. Additionally, since remote sensing is able to provide areal observations, simulations could be improved even in regions, where less or no *in situ* point measurements for initializing the model are available, similar as outlined from (Ottlé et al., 1989). For instance, results indicate a potential need for improving the estimation of the soil hydraulic input parameters during model simulations, since the model was not able to capture dry soil conditions (*i.e.* below 8 vol%), *e.g.* at station US-SRS in Arizona, or overestimated soil moisture values at the dense forest station US-Ho1 in Maine (Fig. 5, Sec. 4.1.). At the dry station US-SRS, the highest deviations between estimated soil moisture profiles and *in situ* measurements are found during extended dry downs with no precipitation event, where the *in situ* measured soil moistures are most variable. Here, high changes in *in situ* measured soil moisture could be found within only a few centimeters of soil (see Sec. 4.1.). This raises the question of how reliable *in situ* soil moisture measurements are, when only few measurements at specific dates are picked out (instead of looking at continuous time series). Further, results at the woody savanna station, US-Ton, showed that static initial model parameters, such as the soil texture, are a strong assumption, which can lead to opposing soil moisture profiles (Fig. 5, 3rd row, Sec. 4.1.). Here, static soil conditions prevent that changes in soil hydraulic properties, due to precipitation or root water uptake, can be captured correctly in HYDRUS-1D model simulations. Not only depend the soil hydraulic properties on soil texture, but several studies showed that soil texture mediates the soil moisture dynamics to some degree (Case and Staver, 2018), and affect the soil moisture retention (Bouma and Bryla, 2000; Sperry and Hacke, 2002). Soil texture composition and its spatio-temporal variability determines how soils response to precipitation events due to its effect on water infiltration and surface runoff. For one, soils with low water permeability (*e.g.* clay soils) are more susceptible to high rates of water runoff, which decreases the available moisture in the soil (Case and Staver, 2018). Second, the study of Sperry and Hacke showed that rather loamy soils can have lower soil water potentials, and hence, lower soil moisture (Dingman, 2015), during summers than rather sandy soils, despite the higher precipitation over the loam site (Sperry and Hacke, 2002). Although, soil types are not that different at employed measuring stations (Fig. 1, Sec. 2.), this finding can be confirmed to some extent at the two in detail investigated stations, US-Ho1 and Stillwater 2 W (see Sec. 4.2.). While at the grassland station Stillwater 2 W the overall precipitation sum during the summer months (1164.9 mm) and the clay percentage (11%) is higher compared to at the forest station US-Ho1 (sum of 1092.8 mm, and 7% of clay), Stillwater 2 W shows overall lower soil moisture profile values (Figs. 5 & 6, Sec. 4.1., Figs. 7 & 8, Sec. 4.2.). In average, during the summer months at Stillwater 2 W, soil moisture profile values of 33.3 vol% are estimated compared to that at US-Ho1 of 46.6 vol%. These results also confirm the influence of vegetation cover on soil moisture profile results, since the influence of soil textures is potentially higher in non-vegetated areas (Gómez-Plaza et al., 2001). Further, studies proved that changes in soil textures over time due to plant and root growth influences how water flows in soils (Fatichi et al., 2020), and hence, affect the soil moisture profiles. In order to improve the performance of the proposed approach, or soil hydraulic models in general, variable soil texture or structure information over time during model simulations should be considered, but can not be realized in common models until now. Additional analyses between *in situ* measurements and the two auxiliary soil moisture products showed that sometimes, the auxiliary products outperform the proposed approach with better statistics. This is true, for example, for the dense forest station US-Ho1 due to the overestimation of retrieved soil moisture values (Fig. 5, Table 6). In the end however, all products showed reasonable results, but the proposed method has the advantage of

continuous determination of soil moisture information with depth without the assumption of non-physical polynomials and is able to provide soil moisture information at depths, where other *in situ* or remote sensing products cannot provide any continuous information with depth (mainly 0–5 cm).

In this study, estimated soil moisture profiles match the local climate and soil conditions. On the one hand, lower soil moisture values are estimated at drier measuring stations, like US-SRS or US-Var, and higher soil moisture values are found at wetter measuring stations, like US-Ho1 (Figs. 5 & 6, Sec. 4.1.). Further, the steepest profile shapes with rather quick changes in soil moisture values across the profile could be found at the driest station, US-SRS in Arizona, as shown in Fig. 4 (see Sec. 4.1.). By contrast, the most uniform profile shapes with less variabilities in soil moisture values across the vertical profile were estimated at the wet and most dense forest station US-Ho1 in Maine. Hence, the statement from (Wu et al., 2002) 'that soil wetness influences how quickly soil wetting/drying moves through the soil column' (Ford et al., 2014) can be confirmed here. On the other hand, analyses regarding average soil moisture profiles for respective dry and wet seasons of the three years (not shown) confirm that during the wet seasons soil moisture is more independent of the soil depth as variabilities across the vertical soil column average out, as demonstrated in (Konings et al., 2014). Further, deeper soil depths have an overall higher persistence of soil moisture than near the surface, as described by (Georgakakos and Bae, 1994), since the highest variabilities are always found in the uppermost part of the soil moisture profiles due to land-atmosphere interactions and feedback. Further, several studies have shown that near-surface and root zone soil moisture are correlated (Ford et al., 2014; Short Gianotti et al., 2019; Akbar et al., 2018). Hence, combining L-band and P-band microwave observations may even advance soil moisture profile approaches and help to analyze the complex link between near-surface and subsurface soil moisture in the future.

6. Conclusions

An approach for estimating continuous soil moisture profiles by combining remotely sensed SAR observations and soil hydraulic model simulations is proposed in this study. The advantages of this approach are, for one, the usage of soil scattering information from remotely sensed SAR observations after the removal of vegetation scattering from the total signal by a polarimetric decomposition. Hence, solely the soil component without influences of the vegetation are employed and no vegetation scattering effects have to be simulated. Second, regarding the soil hydraulic model, a variable set-up of initial assumptions is less prone to model errors. Instead of using just one model realization, as done in standard climate modeling, with potentially false initial assumptions, an ensemble of (realistic) simulations with varying initial assumptions is created, and then compared to actual SAR observations in order to receive the most realistic model set-up and soil moisture profile simulation.

The estimated soil moisture profiles are analyzed in the context of varying climatic and soil conditions as well as validated against several auxiliary soil moisture products (*in situ* measurements, the ERA5-land reanalysis, and the AirMOSS L4). Overall, estimated results agree with satisfying accuracy to *in situ* measurements and other auxiliary products (ERA5-land reanalysis and AirMOSS L4 mission products). The coefficients of determination between estimates and *in situ* values vary between 0.48 and 0.92. The lowest correlations could be found at rather dry desert stations since the employed soil hydraulic model almost always overestimates values. Here, higher correlations might be achieved by improving model initialization parameters, like the soil hydraulic properties, or using non-static soil property information over time. However, the achieved low Fréchet distances, varying between 0.1 and 0.23, showed, that the shape of estimated soil moisture profiles overall fit well to *in situ* measured profiles, what is needed in climate modeling (see Sec. 1.).

In summary, the proposed approach enables the possibility to estimate continuous soil moisture profiles with reasonable shape and accuracy based on remotely sensed observations and hydrological simulations. However, because of the coarse temporal resolution of the AirMOSS SAR observations (recorded from an airplane), no continuous time series analyzes for soil moisture estimations could be performed. Although, theoretically, estimations of timely-dense soil moisture profiles are feasible with this approach, since model simulations can be performed at any temporal scale. Changes in long-term soil moisture profile estimations are important as indicators, *e.g.*, for emerging droughts, with direct impact on agricultural productivity and food security (Almendra-Martín et al., 2021). Further, temporally continuous SAR observations would provide the opportunity to evaluate the performance of the HYDRUS-1D and its ability to capture temporal variations in soil moisture.

The first P-band SAR observations from space will be available from ESA's BIOMASS mission from 2024 onwards with a three-daily repeat pass configuration and 50 m to 200 m resolution (Gelas et al., 2021). As our approach makes use of SAR signals in combination with hydrological simulations, this opens the potential for the assimilation of BIOMASS mission data into hydrological models, using the multilayer SPM as observation operator for comparison with P-band SAR scattering angle observations, to finally update the upper soil states in the prediction step.

Lastly, the proposed approach can be easily used for estimating soil moisture profiles in space. In this study, estimations and analyses are conducted at selected *in situ* measuring stations only since all required input parameters are available from detailed field measurements at high quality, and in order to evaluate the overall performance of the proposed method. However, since remote sensing observations are available over larger areas, only the hydrological model would have to be initialized and driven with the required input parameters in space at comparable spatial resolution. Hence, with this approach the generation of soil moisture profile maps for providing soil moisture information in the horizontal, vertical, and z-direction are possible and will be analyzed in an add-on study.

CRediT authorship contribution statement

Anke Fluhrer: Conceptualization, Data curation, Formal analysis, Investigation, Methodology, Software, Validation, Visualization, Writing – original draft, Writing – review & editing. **Thomas Jagdhuber:** Conceptualization, Funding acquisition, Investigation, Methodology, Project administration, Supervision, Writing – review & editing. **Carsten Montzka:** Funding acquisition, Investigation, Project administration, Supervision, Writing – review & editing. **Maike Schumacher:** Supervision, Writing – review & editing. **Hamed Alemohammad:** Data curation, Resources, Writing – review & editing. **Alireza Tabatabaeenejad:** Software, Writing – review & editing. **Harald Kunstmann:** Investigation, Methodology, Supervision, Writing – review & editing. **Dara Entekhabi:** Methodology, Supervision, Writing – review & editing.

Declaration of competing interest

The authors declare that they have no known competing financial interests or personal relationships that could have appeared to influence the work reported in this paper.

Data availability

The authors do not have permission to share data.

Acknowledgements

This research was funded by the German Federal Ministry for

Economic Affairs and Energy (BMWi) through the German Aerospace Center within the AssimEO project (50EE1914A).

References

Akbar, R., Gianotti, D.S., McColl, K.A., Haghighi, E., Salvucci, G.D., Entekhabi, D., 2018. Hydrological storage length scales represented by remote sensing estimates of soil moisture and precipitation. Water Resour. Res. 54, 1476–1492. https://doi.org/10.1002/2017WR021508.

Alemohammad, S.H., Konings, A.G., Jagdhuber, T., Moghaddam, M., Entekhabi, D., 2018. Characterization of vegetation and soil scattering mechanisms across different biomes using P-band SAR polarimetry. Remote Sens. Environ. 209, 107–117. https://doi.org/10.1016/j.rse.2018.02.032.

Almendra-Martín, L., Martínez-Fernández, J., González-Zamora, Á., Benito-Verdugo, P., Herrero-Jiménez, C.M., 2021. Agricultural drought trends on the Iberian Peninsula: an analysis using modeled and reanalysis soil moisture products. Atmosphere 12, 236. https://doi.org/10.3390/atmos12020236.

AmeriFlux, 2022. https://ameriflux.lbl.gov (accessed on 15 March 2022).

Ashby, S.F., Falgout, R.D., 1996. A parallel multigrid preconditioned conjugate gradient algorithm for groundwater flow simulations. Nucl. Sci. Eng. 124, 145–159. https://doi.org/10.13182/NSE96-A24230.

Bell, J.E., Palecki, M.A., Baker, C.B., Collins, W.G., Lawrimore, J.H., Leeper, R.D., Hall, M.E., Kochendorfer, J., Meyers, T.P., Wilson, T., Diamond, H.J., 2013. U.S. climate reference network soil moisture and temperature observations. J. Hydrometeorol. 14, 977–988. https://doi.org/10.1175/JHM-D-12-0146.1.

Bojinski, S., Verstraete, M., Peterson, T.C., Richter, C., Simmons, A., Zemp, M., 2014. The concept of essential climate variables in support of climate research, applications, and policy. Bull. Am. Meteorol. Soc. 95, 1431–1443. https://doi.org/10.1175/BAMS-D-13-00047.1.

Bouma, T.J., Bryla, D.R., 2000. On the assessment of root and soil respiration for soils of different textures: interactions with soil moisture contents and soil CO2 concentrations. Plant Soil 227, 215–221. https://doi.org/10.1023/A:1026502414977.

Cai, G., Vanderborght, J., Couvreur, V., Mboh, C.M., Vereecken, H., 2018. Parameterization of root water uptake models considering dynamic root distributions and water uptake compensation. Vadose Zone J. 17, 160125 https://doi.org/10.2136/vzj2016.12.0125.

Case, M.F., Staver, A.C., 2018. Soil texture mediates tree responses to rainfall intensity in African savannas. New Phytol. 219, 1363–1372. https://doi.org/10.1111/nph.15254.

Chapin, E., Chau, A., Chen, J., Heavey, B., Hensley, S., Lou, Y., Machuzak, R., Moghaddam, M., 2012. AirMOSS: An airborne P-band SAR to measure root-zone soil moisture. In: 2012 IEEE Radar Conference. Presented at the 2012 IEEE Radar Conference (RadarCon). IEEE, Atlanta, GA, pp. 0693–0698. https://doi.org/10.1109/RADAR.2012.6212227.

Chung, S.-O., Horton, R., 1987. Soil heat and water flow with a partial surface mulch. Water Resour. Res. 23, 2175–2186. https://doi.org/10.1029/WR023i012p02175.

Cloude, S., 2010. Polarisation: Applications in Remote Sensing, 1st ed. Oxford University Press, Oxford, New York.

Crow, W.T., Milak, S., Reichle, R.H., 2016. AirMOSS: L4 Modeled Volumetric Root Zone Soil Moisture, 2012-2015 739558.31901 MB. https://doi.org/10.3334/ORNLDAAC/1421.

Dingman, S.L., 2015. Physical Hydrology, 3. ed. Waveland Press, Long Grove, Ill.

Dirmeyer, P.A., Wu, J., Norton, H.E., Dorigo, W.A., Quiring, S.M., Ford, T.W., Santanello, J.A., Bosilovich, M.G., Ek, M.B., Koster, R.D., Balsamo, G., Lawrence, D. M., 2016. Confronting weather and climate models with observational data from soil moisture networks over the United States. J. Hydrometeorol. 17, 1049–1067. https://doi.org/10.1175/JHM-D-15-0196.1.

Dirmeyer, P.A., Halder, S., Bombardi, R., 2018. On the harvest of predictability from land states in a global forecast model. J. Geophys. Res. Atmos. 123 https://doi.org/10.1029/2018JD029103.

Eiter, T., Mannila, H., 1994. Computing Discrete Fréchet Distance. Technical report CD-TR 94/64. Technical University Vienna.

Etminan, A., Tabatabaeenejad, A., Moghaddam, M., 2020. Retrieving root-zone soil moisture profile from P-band radar via hybrid global and local optimization. IEEE Trans. Geosci. Remote Sensing 58, 5400–5408. https://doi.org/10.1109/TGRS.2020.2965569.

Farthing, M.W., Ogden, F.L., 2017. Numerical solution of Richards' equation: a review of advances and challenges. Soil Sci. Soc. Am. J. 81, 1257–1269. https://doi.org/10.2136/sssaj2017.02.0058.

Fatichi, S., Or, D., Walko, R., Vereecken, H., Young, M.H., Ghezzehei, T.A., Hengl, T., Kollet, S., Agam, N., Avissar, R., 2020. Soil structure is an important omission in earth system models. Nat. Commun. 11, 522. https://doi.org/10.1038/s41467-020-14411-z.

Feddes, Reinder A., Kowalik, Piotr J., Zaradny, Henryk, Feddes, R.A., Kowalik, P.J., Zaradny, H., 1978. Simulation of Field Water Use and Crop Yield, Simulation Monographs. Centre for Agricultural Publishing and Documentation, Wageningen.

Feddes, R.A., Hoff, H., Bruen, M., Dawson, T., de Rosnay, P., Dirmeyer, P., Jackson, R.B., Kabat, P., Kleidon, A., Lilly, A., Pitman, A.J., 2001. Modeling root water uptake in hydrological and climate models. Bull. Amer. Meteor. Soc. 82, 2797–2809. https://doi.org/10.1175/1520-0477(2001)082<2797:MRWUIH>2.3.CO;2.

Fluhrer, A., Jagdhuber, T., Tabatabaeenejad, A., Alemohammad, H., Montzka, C., Friedl, P., Forootan, E., Kunstmann, H., 2022. Remote sensing of complex permittivity and penetration depth of soils using P-band SAR polarimetry. Remote Sens. 14, 2755. https://doi.org/10.3390/rs14122755.

Ford, T.W., Harris, E., Quiring, S.M., 2014. Estimating root zone soil moisture using near-surface observations from SMOS. Hydrol. Earth Syst. Sci. 18, 139–154. https://doi.org/10.5194/hess-18-139-2014.

Fréchet, M., 1906. Sur quelques points du calcul fonctionnel. Rendiconti del Circolo Matematico di Palermo (1884–1940) 22 (1), 1–72.

GDAL/OGR contributors, 2021. GDAL/OGR Geospatial Data Abstraction software Library. Open Source Geospatial Foundation. https://gdal.org.

Gelas, C., Villard, L., Ferro-Famil, L., Polidori, L., Koleck, T., Daniel, S., 2021. Multi-temporal speckle filtering of polarimetric P-band SAR data over dense tropical forests: study case in French Guiana for the BIOMASS Mission. Remote Sens. 13, 142. https://doi.org/10.3390/rs13010142.

Georgakakos, K.P., Bae, D.-H., 1994. Climatic variability of soil water in the American Midwest: Part 2. Spatio-temporal analysis. J. Hydrol. 162, 379–390. https://doi.org/10.1016/0022-1694(94)90237-2.

Gómez-Plaza, A., Martínez-Mena, M., Albaladejo, J., Castillo, V.M., 2001. Factors regulating spatial distribution of soil water content in small semiarid catchments. J. Hydrol. 253, 211–226. https://doi.org/10.1016/S0022-1694(01)00483-8.

He, L., Panciera, R., Tanase, M.A., Walker, J.P., Qin, Q., 2016. Soil moisture retrieval in agricultural fields using adaptive model-based polarimetric decomposition of SAR data. IEEE Trans. Geosci. Remote Sensing 54, 4445–4460. https://doi.org/10.1109/TGRS.2016.2542214.

Hollinger, D., 2021. AmeriFlux US-Ho1 Howland Forest (main tower), Ver. 7-5, AmeriFlux AMP, (dataset). https://doi.org/10.17190/AMF/1246061.

Homeland Infrastructure Foundation-Level Data (HIFLD), 2012. Political Boundaries. https://hifld-geoplatform.opendata.arcgis.com/ [Accessed 06/24/2019].

Homer, C., Dewitz, J., Yang, L., Jin, S., Danielson, P., Xian, G., Coulston, J., Herold, N., Wickham, J., Megown, K., 2015. Completion of the 2011 National Land Cover Database for the conterminous United States-representing a decade of land cover change information. Photogramm. Eng. Remote. Sens. 81, 345–354.

Huang, H., Liao, T.-H., Kim, S.B., Xu, X., Tsang, L., Jackson, T.J., Yueh, S., 2021. L-band radar scattering and soil moisture retrieval of wheat, canola and pasture fields for smap active algorithm. PIER 170, 129–152. https://doi.org/10.2528/PIER21020702.

Jagdhuber, T., 2012. Soil parameter retrieval under vegetation cover using SAR polarimetry. Ph.D. dissertation, Faculty of Science, Univ. Potsdam, Potsdam, Germany, 2012 [Online]. Available: http://opus.kobv.de/ubp/volltexte/2012/6051/.

Jagdhuber, T., Hajnsek, I., Papathanassiou, K.P., 2015. An iterative generalized hybrid decomposition for soil moisture retrieval under vegetation cover using fully polarimetric SAR. IEEE J. Sel. Top. Appl. Earth Observ. Remote Sensing 8, 3911–3922. https://doi.org/10.1109/JSTARS.2014.2371468.

Kim, S.-B., Liao, T.-H., 2021. Robust retrieval of soil moisture at field scale across wide-ranging SAR incidence angles for soybean, wheat, forage, oat and grass. Remote Sens. Environ. 266, 112712 https://doi.org/10.1016/j.rse.2021.112712.

Konings, A.G., Entekhabi, D., Moghaddam, M., Saatchi, S.S., 2014. The effect of variable soil moisture profiles on P-band backscatter. IEEE Trans. Geosci. Remote Sensing 52, 6315–6325. https://doi.org/10.1109/TGRS.2013.2296035.

Koster, R.D., Mahanama, S.P.P., Yamada, T.J., Balsamo, G., Berg, A.A., Boisserie, M., Dirmeyer, P.A., Doblas-Reyes, F.J., Drewitt, G., Gordon, C.T., Guo, Z., Jeong, J.-H., Lee, W.-S., Li, Z., Luo, L., Malyshev, S., Merryfield, W.J., Seneviratne, S.I., Stanelle, T., van den Hurk, B.J.J.M., Vitart, F., Wood, E.F., 2011. The second phase of the global land–atmosphere coupling experiment: soil moisture contributions to subseasonal forecast skill. J. Hydrometeorol. 12, 805–822. https://doi.org/10.1175/2011JHM1365.1.

Law, B., 2021. AmeriFlux US-Me6 Metolius Young Pine Burn, Ver. 15-5, AmeriFlux AMP, (Dataset). https://doi.org/10.17190/AMF/1246128.

Lei, F., Crow, W.T., Kustas, W.P., Dong, J., Yang, Y., Knipper, K.R., Anderson, M.C., Gao, F., Notarnicola, C., Greifeneder, F., McKee, L.M., Alfieri, J.G., Hain, C., Dokoozlian, N., 2020. Data assimilation of high-resolution thermal and radar remote sensing retrievals for soil moisture monitoring in a drip-irrigated vineyard. Remote Sens. Environ. 239, 111622 https://doi.org/10.1016/j.rse.2019.111622.

Liu, Q., Reichle, R.H., Bindlish, R., Cosh, M.H., Crow, W.T., de Jeu, R., De Lannoy, G.J. M., Huffman, G.J., Jackson, T.J., 2011. The contributions of precipitation and soil moisture observations to the skill of soil moisture estimates in a land data assimilation system. J. Hydrometeorol. 12, 750–765. https://doi.org/10.1175/JHM-D-10-05000.1.

Lucas, R.M., Moghaddam, M., Cronin, N., 2004. Microwave scattering from mixed-species forests, Queensland, Australia. IEEE Trans. Geosci. Remote Sensing 42, 2142–2159. https://doi.org/10.1109/TGRS.2004.834633.

Ma, S., Xu, L., Verfaillie, J., Baldocchi, D., 2021. AmeriFlux US-Ton Tonzi Ranch, Ver. 13-5, AmeriFlux AMP, (Dataset). https://doi.org/10.17190/AMF/1245971.

Ma, S., Xu, L., Verfaillie, J., Baldocchi, D., 2022. AmeriFlux US-Var Vaira ranch- Ione, Ver. 15-5, AmeriFlux AMP, (Dataset). https://doi.org/10.17190/AMF/1245984.

Maity, R., 2022. Statistical Methods in Hydrology and Hydroclimatology, Second, edition. ed. Springer transactions in civil and environmental engineering, Springer, Singapore.

Mironov, V.L., Kosolapova, L.G., Fomin, S.V., 2009. Physically and mineralogically based spectroscopic dielectric model for moist soils. IEEE Trans. Geosci. Remote Sensing 47, 2059–2070. https://doi.org/10.1109/TGRS.2008.2011631.

Moghaddam, M., Saatchi, S., 1995. Analysis of scattering mechanisms in SAR imagery over boreal forest: results from BOREAS '93. IEEE Trans. Geosci. Remote Sensing 33, 1290–1296. https://doi.org/10.1109/36.469495.

Moghaddam, M., Tabatabaeenejad, A., Chen, R.H., Saatchi, S., Jaruwatanadilok, S., Burgin, M., Duan, X., Truong-Loi, M.L., 2016. AirMOSS: L2/3 Volumetric Soil Moisture Profiles Derived From Radar, 2012-2015 2551.326499 MB. https://doi.org/10.3334/ORNLDAAC/1418.

Mualem, Y., 1976. A new model for predicting the hydraulic conductivity of unsaturated porous media. Water Resour. Res. 12, 513–522. https://doi.org/10.1029/WR012i003p00513.

Muñoz Sabater, J., 2019. ERA5-Land hourly data from 1981 to present. Copernicus Climate Change Service (C3S) Climate Data Store (CDS) (Accessed on 10-08-2022). https://doi.org/10.24381/CDS.E2161BAC.

Muñoz-Sabater, J., Dutra, E., Agustí-Panareda, A., Albergel, C., Arduini, G., Balsamo, G., Boussetta, S., Choulga, M., Harrigan, S., Hersbach, H., Martens, B., Miralles, D.G., Piles, M., Rodríguez-Fernández, N.J., Zsoter, E., Buontempo, C., Thépaut, J.-N., 2021. ERA5-Land: a state-of-the-art global reanalysis dataset for land applications. Earth Syst. Sci. Data 13, 4349–4383. https://doi.org/10.5194/essd-13-4349-2021.

Nakhaei, M., Šimůnek, J., 2014. Parameter estimation of soil hydraulic and thermal property functions for unsaturated porous media using the HYDRUS-2D code. J. Hydrol. Hydromech. 62, 7–15. https://doi.org/10.2478/johh-2014-0008.

Nauman, T., Ramcharan, A., Brungard, C., Thompson, J., Wills, S., Waltman, S., Hengl, T., 2017. Soil Properties and Class 100m Grids United States. https://doi.org/10.18113/S1KW2H.

Orgogozo, L., Renon, N., Soulaine, C., Hénon, F., Tomer, S.K., Labat, D., Pokrovsky, O.S., Sekhar, M., Ababou, R., Quintard, M., 2014. An open source massively parallel solver for Richards equation: mechanistic modelling of water fluxes at the watershed scale. Comput. Phys. Commun. 185, 3358–3371. https://doi.org/10.1016/j.cpc.2014.08.004.

Ottlé, C., Vidal-Madjar, D., Girard, G., 1989. Remote sensing applications to hydrological modeling. J. Hydrol. 105, 369–384. https://doi.org/10.1016/0022-1694(89)90114-5.

Peel, M.C., Finlayson, B.L., McMahon, T.A., 2007. Updated world map of the Köppen-Geiger climate classification. Hydrol. Earth Syst. Sci. 11, 1633–1644. https://doi.org/10.5194/hess-11-1633-2007.

QGIS Development Team, 2021. QGIS Geographic Information System. Open Source Geospatial Foundation Project. http://qgis.osgeo.org.

Reichle, R.H., De Lannoy, G.J.M., Liu, Q., Ardizzone, J.V., Colliander, A., Conaty, A., Crow, W., Jackson, T.J., Jones, L.A., Kimball, J.S., Koster, R.D., Mahanama, S.P., Smith, E.B., Berg, A., Bircher, S., Bosch, D., Caldwell, T.G., Cosh, M., González-Zamora, Á., Holifield Collins, C.D., Jensen, K.H., Livingston, S., Lopez-Baeza, E., Martínez-Fernández, J., McNairn, H., Moghaddam, M., Pacheco, A., Pellarin, T., Prueger, J., Rowlandson, T., Seyfried, M., Starks, P., Su, Z., Thibeault, M., van der Velde, R., Walker, J., Wu, X., Zeng, Y., 2017. Assessment of the SMAP Level-4 surface and root-zone soil moisture product using in situ measurements. J. Hydrometeorol. 18, 2621–2645. https://doi.org/10.1175/JHM-D-17-0063.1.

Rizzoli, P., Martone, M., Gonzalez, C., Wecklich, C., Borla Tridon, D., Bräutigam, B., Bachmann, M., Schulze, D., Fritz, T., Huber, M., Wessel, B., Krieger, G., Zink, M., Moreira, A., 2017. Generation and performance assessment of the global TanDEM-X digital elevation model. ISPRS J. Photogramm. Remote Sens. 132, 119–139. https://doi.org/10.1016/j.isprsjprs.2017.08.008.

Sadeghi, M., Tabatabaeenejad, A., Tuller, M., Moghaddam, M., Jones, S., 2016. Advancing NASA's AirMOSS P-band radar root zone soil moisture retrieval algorithm via incorporation of Richards' equation. Remote Sens. 9, 17. https://doi.org/10.3390/rs9010017.

Sandrock, C., Afshari, S., 2016. alchemyst/ternplot: DOI version (v1.1.0). Zenodo [Accessed 05/15/2020]. Zenodo. https://doi.org/10.5281/ZENODO.166760.

Sato, A., Yamaguchi, Y., Singh, G., Park, Sang-Eun, 2012. Four-component scattering power decomposition with extended volume scattering model. IEEE Geosci. Remote Sensing Lett. 9, 166–170. https://doi.org/10.1109/LGRS.2011.2162935.

Shi, Y., Davis, K.J., Duffy, C.J., Yu, X., 2013. Development of a coupled land surface hydrologic model and evaluation at a critical zone observatory. J. Hydrometeorol. 14, 1401–1420. https://doi.org/10.1175/JHM-D-12-0145.1.

Short Gianotti, D.J., Salvucci, G.D., Akbar, R., McColl, K.A., Cuenca, R., Entekhabi, D., 2019. Landscape water storage and subsurface correlation from satellite surface soil moisture and precipitation observations. Water Resour. Res. 55, 9111–9132. https://doi.org/10.1029/2019WR025332.

Šimůnek, J., Šejna, M., Saito, H., Sakai, M., Van Genuchten, M.Th., 2013. The HYDRUS-1D software package for simulating the one-dimensional movement of water, heat, and multiple solutes in variably-saturated media (Manual Version 4.17). Riverside, California.

Sperry, J.S., Hacke, U.G., 2002. Desert shrub water relations with respect to soil characteristics and plant functional type: *desert shrub water relations*. Funct. Ecol. 16, 367–378. https://doi.org/10.1046/j.1365-2435.2002.00628.x.

Tabatabaeenejad, A., Moghaddam, M., 2006. Bistatic scattering from three-dimensional layered rough surfaces. IEEE Trans. Geosci. Remote Sensing 44, 2102–2114. https://doi.org/10.1109/TGRS.2006.872140.

Tabatabaeenejad, A., Burgin, M., Duan, Xueyang, Moghaddam, M., 2015. P-band radar retrieval of subsurface soil moisture profile as a second-order polynomial: first AirMOSS results. IEEE Trans. Geosci. Remote Sensing 53, 645–658. https://doi.org/10.1109/TGRS.2014.2326839.

Tangdamrongsub, N., Han, S.-C., Yeo, I.-Y., Dong, J., Steele-Dunne, S.C., Willgoose, G., Walker, J.P., 2020. Multivariate data assimilation of GRACE, SMOS, SMAP measurements for improved regional soil moisture and groundwater storage estimates. Adv. Water Resour. 135, 103477 https://doi.org/10.1016/j.advwatres.2019.103477.

Tóth, B., Weynants, M., Nemes, A., Makó, A., Bilas, G., Tóth, G., 2015. New generation of hydraulic pedotransfer functions for Europe: new hydraulic pedotransfer functions for Europe. Eur. J. Soil Sci. 66, 226–238. https://doi.org/10.1111/ejss.12192.

van Zyl, J.J., Arii, M., Kim, Y., 2011. Model-based decomposition of polarimetric SAR covariance matrices constrained for nonnegative eigenvalues. IEEE Trans. Geosci. Remote Sensing 49, 3452–3459. https://doi.org/10.1109/TGRS.2011.2128325.

Vereecken, H., Amelung, W., Bauke, S.L., Bogena, H., Brüggemann, N., Montzka, C., Vanderborght, J., Bechtold, M., Blöschl, G., Carminati, A., Javaux, M., Konings, A.G., Kusche, J., Neuweiler, I., Or, D., Steele-Dunne, S., Verhoef, A., Young, M., Zhang, Y., 2022. Soil hydrology in the Earth system. Nat Rev Earth Environ 3, 573–587. https://doi.org/10.1038/s43017-022-00324-6.

Vivoni, E., 2022. AmeriFlux US-SRS Santa Rita Experimental Range Mesquite Savanna, Ver. 3-5, AmeriFlux AMP, (Dataset). https://doi.org/10.17190/AMF/1660351.

Walker, J.P., Willgoose, G.R., Kalma, J.D., 2001. One-dimensional soil moisture profile retrieval by assimilation of near-surface observations: a comparison of retrieval algorithms. Adv. Water Resour. 24, 631–650. https://doi.org/10.1016/S0309-1708(00)00043-9.

World Meteorological Organization, 2021. Comission for Observation, Infrastructure And Information Systems, Abridged Final Report of the First Session, WMO-No. 1251.

Wu, W., Geller, M.A., Dickinson, R.E., 2002. The response of soil moisture to long-term variability of precipitation. J. Hydrometeorol. 3, 604–613.